hydrology

MDPI

Article

GWBASE: An Algorithm for Screening Groundwater–Baseflow Coupling Using Paired USGS Well and Streamflow Records

Xueyi Li [1], Norman L. Jones [1,*], Gustavious P. Williams [1], Amin Aghababaei [1], Riley C. Hales [1], Eniola Webster-Esho [2], Ryan van der Heijden [3], T. Prabhakar Clement [2] and Donna M. Rizzo [3]

[1] Civil and Construction Engineering, Brigham Young University, Provo, UT 84602, USA; xueyil@student.byu.edu (X.L.); gus.p.williams@byu.edu (G.P.W.); aghababa@student.byu.edu (A.A.); rchales@byu.edu (R.C.H.)
[2] Civil, Construction, and Environmental Engineering, University of Alabama, Tuscaloosa, AL 35487, USA; ewebsteresho@crimson.ua.edu (E.W.-E.); pclement@ua.edu (T.P.C.)
[3] Civil and Environmental Engineering, University of Vermont, Burlington, VT 05405, USA; rvanderh@uvm.edu (R.v.d.H.); drizzo@uvm.edu (D.M.R.)
* Correspondence: njones@byu.edu; Tel.: +1-801-422-7569

Abstract

Groundwater discharge contributes to stream baseflow, but coupling strength varies among catchments and transferable quantification methods are limited. We present GWBASE, an open-source Python algorithm that pairs U.S. Geological Survey (USGS) wells and gages within hydrographic catchments and ranks coupling at each gage by linear regression and mutual information (MI, capturing nonlinear and lagged dependence) on monthly ΔWTE–ΔQ records from baseflow-dominated months. We apply it to the Great Salt Lake Basin (Utah; ~93,000 km^2 with 8752 USGS wells, 1906–2025). GWBASE ranked four terminal-gage catchments using a seasonally corrected, within-well regression as the primary estimate; three of the four show statistically significant groundwater–baseflow coupling. The ranking depends on the metric: absolute magnitude (cfs per foot) is dominated by the large Bear River catchment, whereas size-normalized sensitivity and coupling tightness identify the smaller Little Cottonwood Creek. The basin-scale aggregate (~4 cfs per foot of basin-averaged decline) is dominated by Bear River and, once catchment-level uncertainty is propagated, is not distinguishable from zero. Because national groundwater records are predominantly intermittent, GWBASE resolves seasonal-to-interannual storage coupling rather than event-scale exchange. It is best used for screening and ranking catchment-scale coupling rather than yielding a single basin-scale coefficient.

Keywords: groundwater; baseflow; groundwater–surface water interaction; mutual information; Great Salt Lake Basin

Check for updates

Academic Editors: Kristine Walraevens, Alemu Yenehun and Adugnaw Birhanu

Received: 20 June 2026
Revised: 6 August 2026
Accepted: 27 August 2026
Published: 30 August 2026

Copyright: © 2026 by the authors. Licensee MDPI, Basel, Switzerland. This article is an open access article distributed under the terms and conditions of the Creative Commons Attribution (CC BY) license.

1. Introduction

Baseflow is the portion of streamflow sustained between storm events by the slow release of stored water, from both bankflow and deeper groundwater directly or from seeps and springs. During dry periods, when quickflow from recent precipitation has receded, baseflow becomes the sole source of streamflow. The exchange between aquifer and channel, however, is not one-directional: where the water table exceeds the stream stage, the reach is *gaining* and groundwater discharges to the channel as baseflow, but where the water table falls below the streambed, the reach becomes *losing* and streamflow is lost to the aquifer [1]. Declining water tables can both reduce baseflow and shift a reach from gaining to losing

conditions. Baseflow sustains hydrologic connectivity, aquatic habitat, and water quality, and because it directly reflects groundwater storage and discharge, its variability serves as a sensitive indicator of watershed condition under changing climate and land use.

Groundwater is a primary source of baseflow in many basins, particularly where water tables are shallow and aquifer materials are permeable [1]. Field and conceptual studies show that reductions in groundwater storage, e.g., declining water tables, limit aquifer discharge to streams during rain-free periods, reducing baseflow [2,3]. This mechanism operates across diverse settings: in mountain headwaters, declining groundwater storage amplifies warm-season streamflow reductions under warming [4], while in heavily pumped agricultural basins, groundwater depletion is linked to persistent summer low-flow declines and increased streamflow intermittency [5–7]. These concerns are reinforced by widespread and accelerating groundwater depletion. Jasechko et al. [8] report rapid groundwater declines across most monitored aquifers worldwide, and Famiglietti [9] characterizes the cumulative trend as a global crisis with consequences for streamflow, food security, and ecosystem function. In the United States, the Central Valley and High Plains aquifers in particular have lost storage at rates that exceed natural recharge [10], and declining water levels have been documented across major aquifer systems [11] and in recent national assessments [7,12]. The trend is not universal, however: in parts of West Africa, including the Sahel, groundwater storage has increased rather than declined [13,14].

The conceptual basis for groundwater–surface water (GW–SW) interaction is well established. Winter et al. [1] frame groundwater and surface water as components of a single, connected resource, and Barlow and Leake [3] provide an analytical framework for streamflow depletion induced by groundwater pumping. Process-based studies emphasize that this coupling varies in strength and timing depending on hydrogeology, climate, and groundwater withdrawals [15].

At the catchment scale, recession analysis [16] and digital-filter baseflow separation [17] have been widely used to partition streamflow into baseflow and quickflow components and to infer aquifer storage behavior. However, these approaches generally infer groundwater contributions from recessional streamflow alone and do not directly compare groundwater-level observations against changes in observed streamflow. Such comparisons are only meaningful when streamflow is dominated by baseflow, because during quickflow-dominated periods, surface processes mask the groundwater signal. As a result, the groundwater–streamflow relationship can only be reliably resolved when streamflow is primarily sustained by groundwater discharge.

The U.S. Geological Survey (USGS) maintains national networks of stream gages and groundwater wells that provide decades of concurrent observations—daily streamflow and intermittent groundwater levels—across diverse hydroclimatic and geologic settings. These records make it possible to assess groundwater–baseflow relationships systematically and at regional scales without relying on local field campaigns or site-specific models. Despite these data availability, quantitative and generalizable methods for diagnosing groundwater–baseflow coupling directly from paired well and gage records remain limited. Existing approaches tend to fall into three categories: (a) small-N case studies focused on individual watersheds [18], (b) basin-specific numerical models that require local calibration [4,6], or (c) regional assessments of groundwater storage change that do not isolate the baseflow component of streamflow [8,10].

The objective of this study is to develop a generalized, transferable algorithm that uses paired USGS well and gage observations to identify a groundwater-influenced baseflow signal and quantify the strength of groundwater–streamflow coupling across catchments. Building on a machine learning classifier that labels each daily streamflow observation as baseflow-dominated or not [19], the algorithm is designed to (1) pair wells and gages

and identify hydrologically connected catchments, (2) quantify and rank coupling strength at each gage, and (3) characterize nonlinear and lagged relationships using a mutual-information metric in addition to linear regression. We implement this algorithm in an open-source Python package called GWBASE, and demonstrate it on the Great Salt Lake Basin. The results show that absolute and size-normalized coupling metrics yield different catchment rankings, highlighting the importance of evaluating groundwater–baseflow interactions from multiple complementary perspectives.

2. Materials and Methods

2.1. Study Area

Although this paper focuses primarily on the GWBASE algorithm, we demonstrate its application and utility in the Great Salt Lake Basin (GSLB) in Utah (Figure 1). This case study provides context for discussing capabilities, challenges, and methods for performing studies of streamflow–groundwater interactions. The GSLB has an area of approximately 93,000 km^2 across northern Utah and adjacent portions of Idaho, Wyoming, and Nevada, and is comprised of five sub-basins: the Bear River, Weber River, Jordan River, Utah Lake, and West Desert drainages [20]. It is a closed hydrologic system, in which all surface water drains toward the Great Salt Lake with no outlet to the ocean. This means that each basin has a terminal gage near the inflow to the lake. Streamflow is supplied mainly by snowmelt-fed rivers originating in the Wasatch and Uinta Mountains, while diversions and evaporation account for most losses. Annual precipitation ranges from roughly 10–65 cm in the low-elevation valleys to more than 100 cm in the surrounding mountain headwaters [21], producing strong hydroclimatic gradients and sustained groundwater–surface water exchange.

Groundwater resources in the basin occur primarily within two broad hydrogeologic settings: unconsolidated basin-fill deposits along the Wasatch Front, the Bear River, and Utah Lake basins, and consolidated bedrock formations in the surrounding ranges [22,23]. The unconsolidated basin fill—largely derived from Lake Bonneville lacustrine sediments interbedded with coarse alluvial and deltaic units—forms the most productive aquifers, with locally confined, unconfined, and perched conditions [22]. Basin-and-range faulting further compartmentalizes the system. Together, these basin-fill and bedrock aquifers form an interconnected system that controls regional groundwater storage and discharge to streams.

Population growth along the Wasatch Front has placed increasing pressure on regional water resources. Salt Lake County in the Jordan River sub-basin is projected to grow from roughly 0.9 million residents in 2000 to about 2 million by 2060, with the population in the Utah Lake Basin nearly tripling over the same period [24,25]. Groundwater in the GSLB is withdrawn chiefly for municipal water supply, irrigated agriculture, industry, and domestic and livestock use [22]. Concern over water resources and supply has intensified with record-low Great Salt Lake levels [20,26]. Recent studies document substantial basin-scale groundwater storage losses during the 2011–2016 and 2019–2022 droughts: GPS-based deformation analysis indicates approximately 10 km^3 of groundwater loss during the 2011–2016 drought alone [27], and a companion study using GRACE, GLDAS, and in situ observations confirms two major drawdown intervals with only partial recovery [28]. At the broader GSLB scale, snowfall during wet years can partially replenish groundwater storage but does not offset the long-term trend toward aridification [29]. These storage-scale findings motivate the present study's focus on the linked baseflow response.

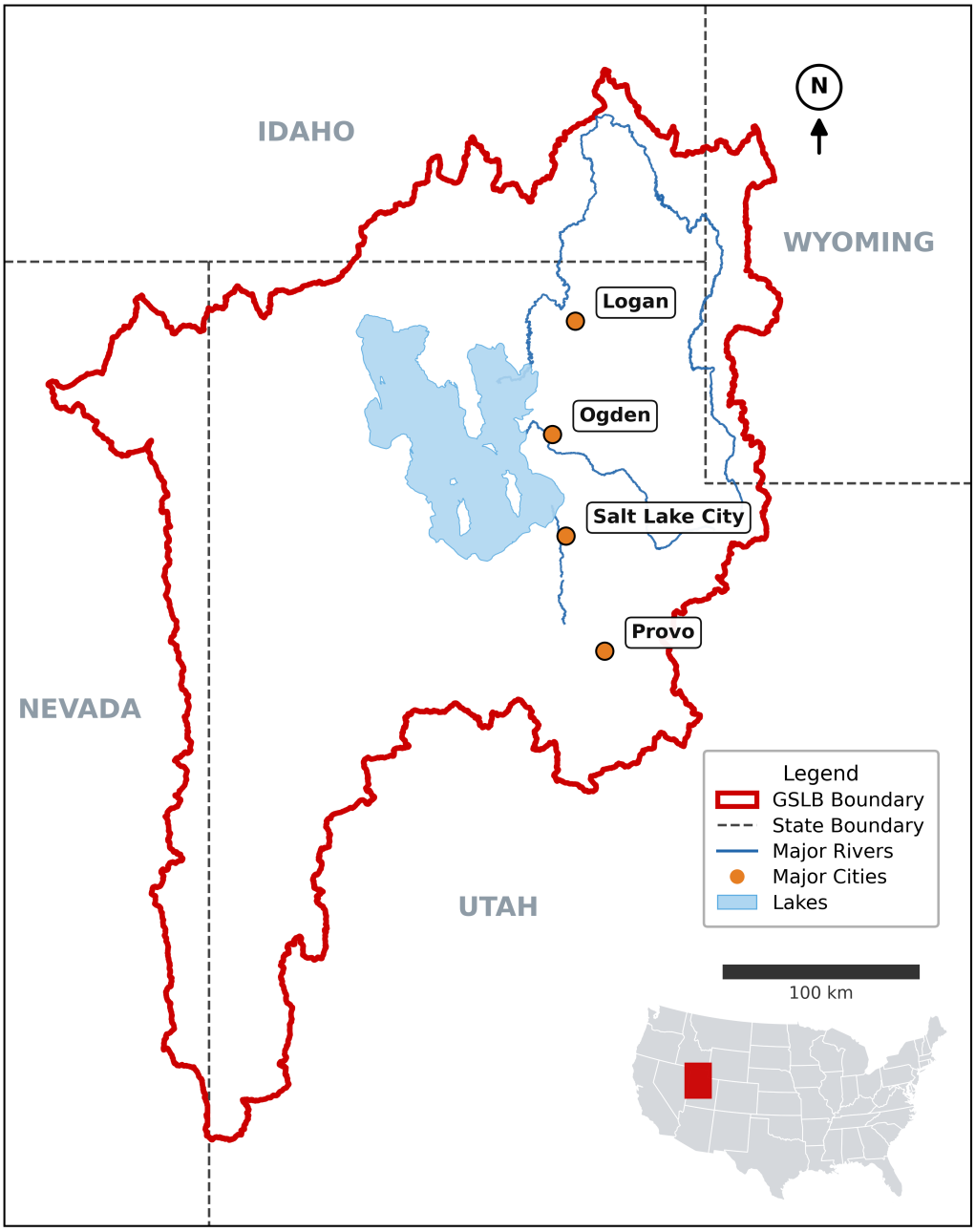

Figure 1. Great Salt Lake Basin (GSLB) study area.

2.2. Data

This study uses data from three national-scale sources: daily streamflow records from the USGS stream gage network, groundwater level observations from the USGS National Water Information System (NWIS) [30], and stream-network and catchment boundaries from the Group on Earth Observations (GEO) Global Water Sustainability (GEOGLOWS) dataset [31]. Stream gages provide data we used to identify baseflow-dominated periods, while groundwater wells provide water-table elevation (WTE) observations for comparison with streamflow.

2.2.1. Groundwater Level Data

We obtained groundwater-level data from the NWIS [30], a national repository of long-term records from over 850,000 monitoring wells across the United States. Each record reports well location, land-surface elevation, and depth-to-water. We convert depth-to-

water values to a water-table elevation (WTE) value that is referenced to mean sea level by subtracting depth-to-water from the land-surface elevation.

Within the GSLB, 8752 wells have usable water-level records spanning 1906–2025, comprising both continuously monitored and intermittently sampled wells. Figure 2 shows the spatial distribution of the wells, with the higher densities in the populated valley lowlands and sparsest coverage in the surrounding mountains.

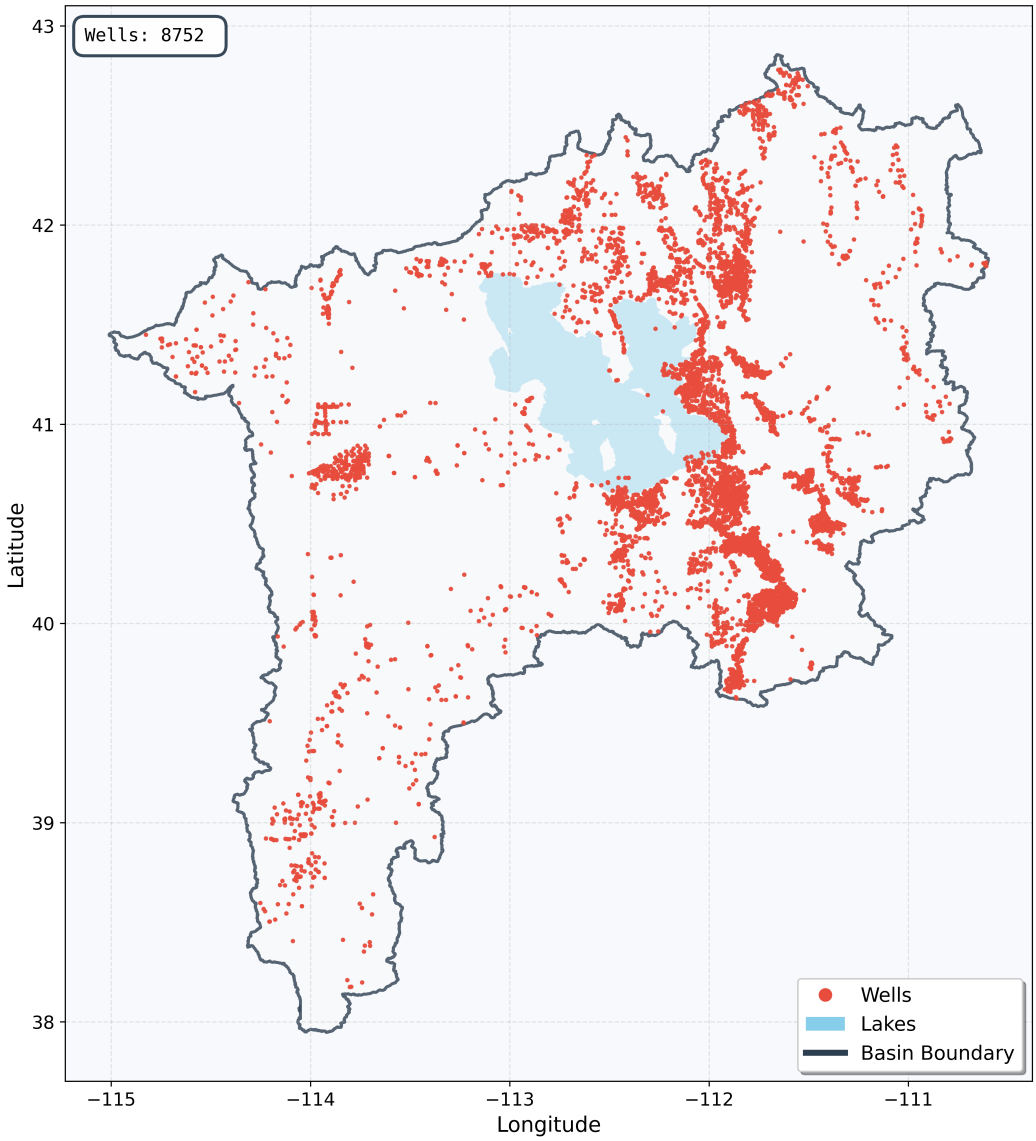

Figure 2. Spatial distribution of the 8752 USGS groundwater wells with usable water-level records across the Great Salt Lake Basin. Well density is highest in the valley regions and sparse in the surrounding uplands.

2.2.2. Streamflow Data and Gage Information

We obtained daily streamflow data from the NWIS [32]. We excluded stream gages with insufficient temporal coverage. We linked the remaining gage locations to their closest corresponding stream reaches from the National Water Model hydrofabric (i.e., stream network) [33]. This linkage allows us to pair a gage with its corresponding stream reach and supports gage selection and spatial pairing with groundwater wells in each sub-basin.

2.2.3. Hydrography Data

We obtained the stream network and catchment boundaries from the GEOGLOWS dataset, which provides globally consistent hydrologic features [31]. The GEOGLOWS stream network represents the global river system as a connected set of stream reaches, each with a unique identifier, geometric attributes, and explicit upstream–downstream connectivity. Corresponding catchment polygons delineate the contributing drainage area for each stream reach.

Figure 3 presents the spatial layout of major streams and catchments used in this study.

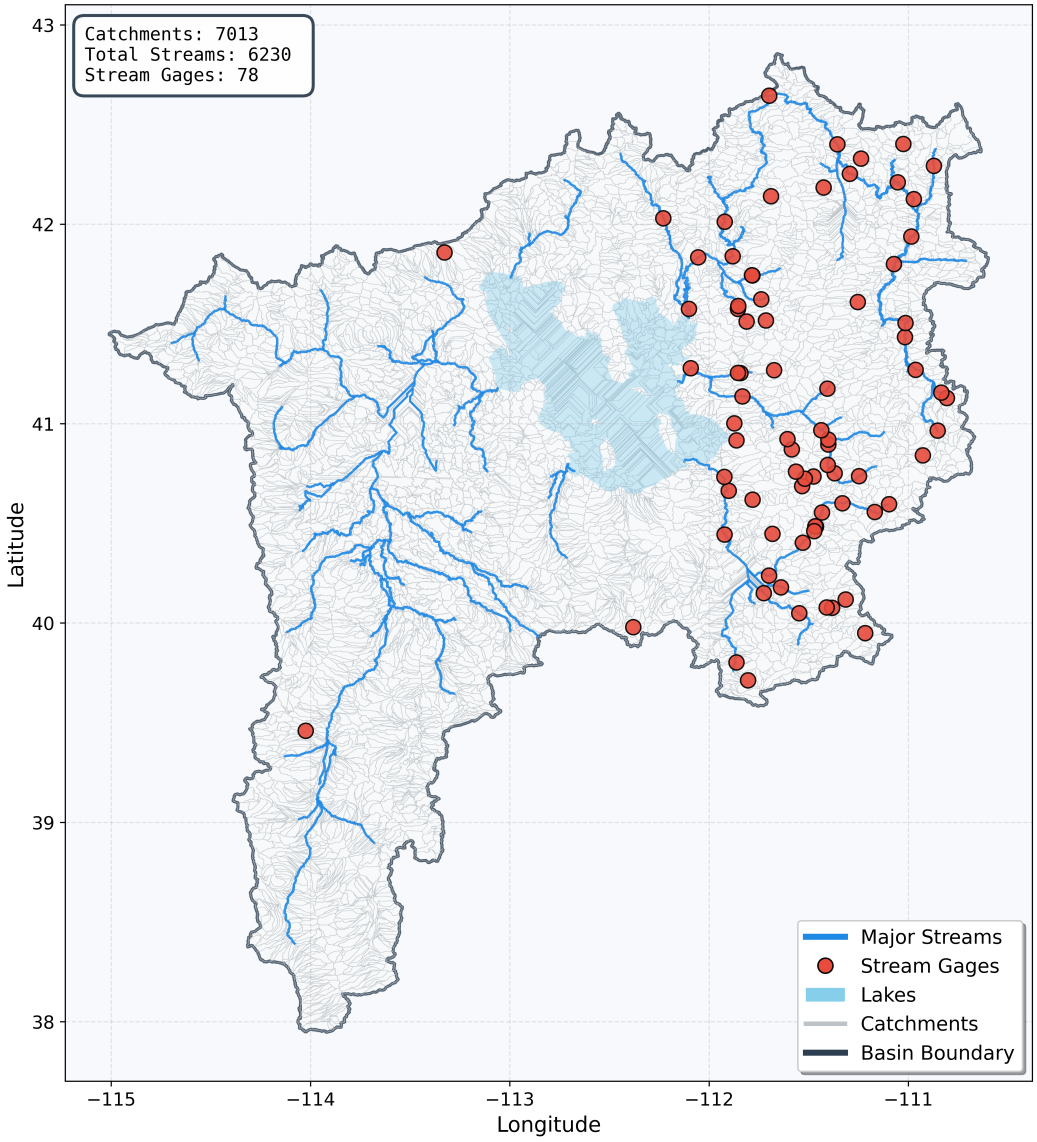

Figure 3. Stream network and catchment boundaries for the Great Salt Lake Basin, derived from the GEOGLOWS hydrographic dataset and used for well–gage pairing. GEOGLOWS routing continuations that crossed the lake polygon to preserve upstream–downstream topology (not real channels) have been masked, except for the reach draining into Bear River Bay, which is a genuine lake-draining outlet.

2.3. Algorithm Overview

We developed an algorithm to quantify and characterize the relationship between groundwater-level change and streamflow change during baseflow-dominated (BFD) periods. We implemented it in a Python 3.10 package called GWBASE [34]. The GWBASE workflow (Figure 4) consists of nine sequential steps, each described below and grouped into four phases: pairing, filtering and interpolation, paired-record construction, and statistical analysis.

The algorithm timescale is set by the timescale of the observations. Groundwater levels in the national monitoring network are predominantly intermittent manual measurements, so the workflow interpolates them to monthly resolution (Step 5) rather than finer. GWBASE, as implemented with monthly time steps, resolves seasonal-to-interannual storage coupling rather than event-scale exchange. We examine the implications of this timescale limitation in Section 4.4.

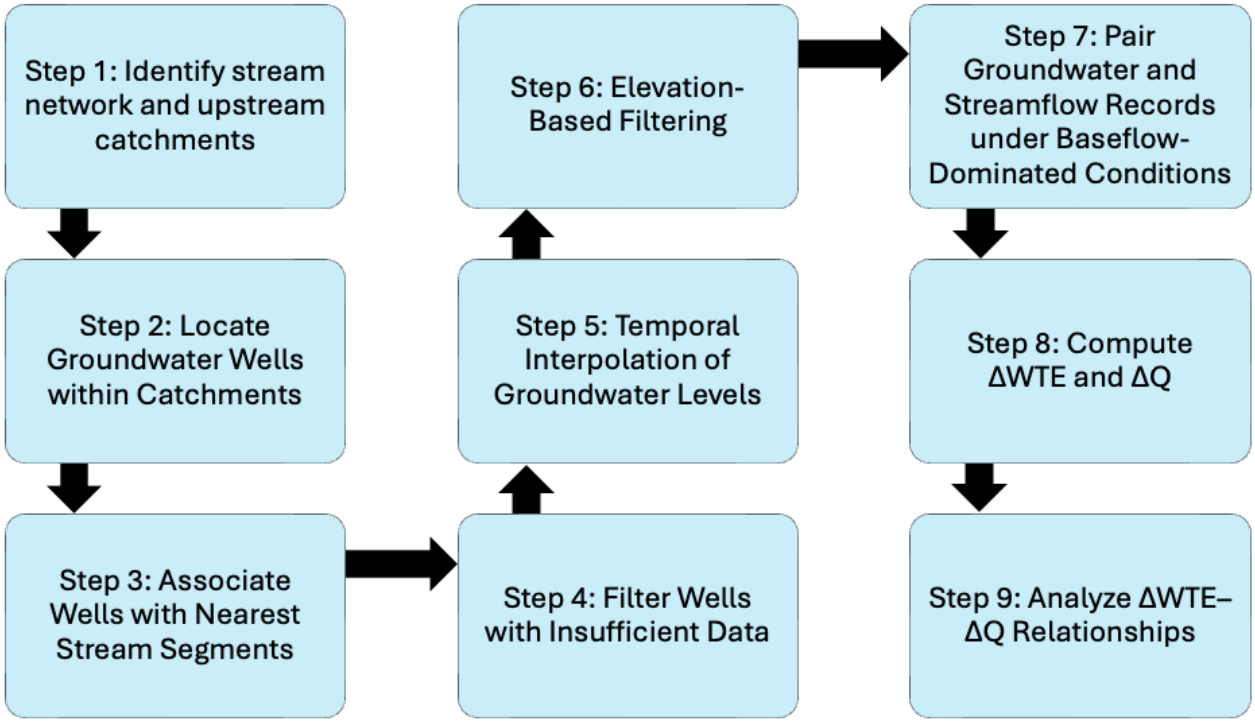

Figure 4. Overview of the GWBASE workflow as nine sequential steps, from identifying the stream network and pairing wells with gages (Steps 1–3), through filtering and temporal interpolation of groundwater levels (Steps 4–6), to constructing paired water-level-change versus baseflow-change records (ΔWTE–ΔQ; Steps 7–8) and analyzing their relationship (Step 9).

2.4. Baseflow-Dominated Day Classification

Because GWBASE analyzes streamflow only when it is groundwater-fed (i.e., BFD conditions), the workflow first classifies the flow on each day as BFD or not. For the case study, we apply a previously developed machine learning classifier [19] to the daily streamflow series, assigning BFD = 1 when streamflow is primarily baseflow (little or no quickflow) and BFD = 0 otherwise. The classifier was trained on hand-labeled streamflow records using hydrologically relevant features, and its performance and validation were reported in the original study. All subsequent analyses are restricted to BFD = 1 days (Figure 5).

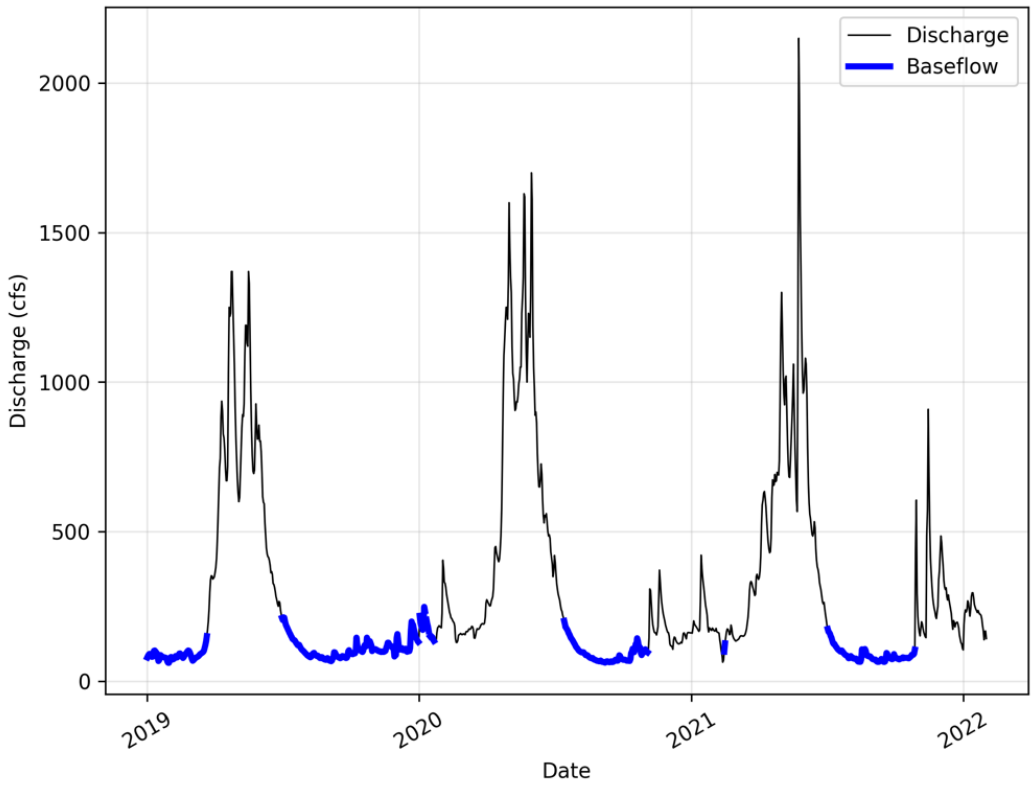

Figure 5. Example streamflow hydrograph showing baseflow-dominated days (BFD = 1), highlighted in blue, and non-baseflow days (BFD = 0). The highlighted segments are the observed discharge on days the classifier labels baseflow-dominated; they are not a separated baseflow component. A linear discharge axis is used deliberately, so that the contrast between snowmelt peaks and the baseflow recessions between them remains visible.

2.5. Algorithm Steps

Using BFD-classified streamflow data, the GWBASE workflow proceeds through the nine steps and phases shown in Figure 4. We describe each step in turn below.

2.5.1. Step 1: Identify Stream Network and Upstream Catchments

The GWBASE workflow first matches each stream gage with the catchment that contains it by mapping gage coordinates to GEOGLOWS catchment polygons, establishing gage–catchment relationships. Because multiple gages often lie along the same flow path, analyzing each independently would duplicate upstream drainage areas. To avoid this, each drainage network is reduced to a single *terminal gage*, defined as a gage with no other gage downstream of it in a given catchment.

We identify terminal gages by representing the stream network as a directed graph from its connectivity fields, where the upstream catchment ID (LINKNO) and downstream link (DSLINKNO) define the graph edges. A gage is classified as terminal if no downstream path leads to another gage. We performed a manual review step to correct edge cases that the automated rule misses—gages on diversions, gages at shared outlets, and gages spanning multiple independent drainage divides.

For each terminal gage, the GWBASE workflow delineates the complete upstream contributing area by tracing all connected upstream catchments, producing non-overlapping drainage regions used for subsequent analysis. These regions define the spatial units used for the well–gage pairing in Step 2.

Figure 6 shows a schematic example of this accumulation.

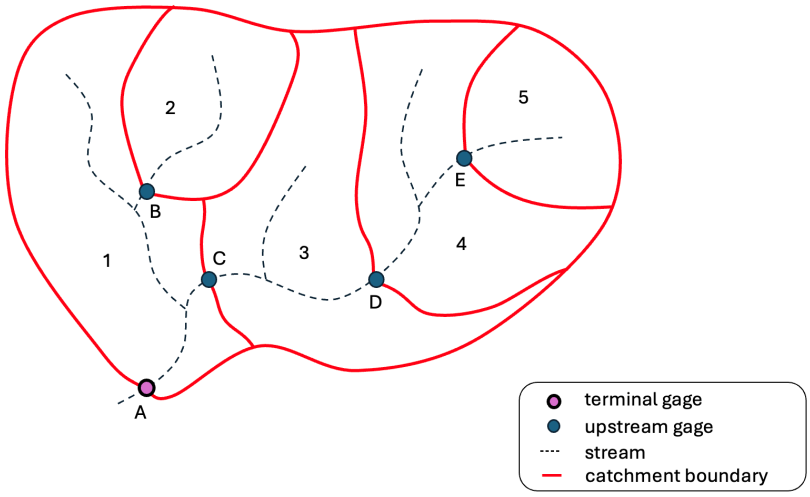

Figure 6. Example drainage network showing terminal and upstream gages, local catchments, and streamflow direction used to delineate contributing areas. Numbered polygons (1–5) are the local catchments draining to each gage; lettered points (A–E) are the gages, with A the terminal gage; dashed curves are stream reaches.

2.5.2. Step 2: Locate Groundwater Wells Within Catchments

GWBASE assigns groundwater wells to terminal gages using a point-in-polygon spatial join, linking each well to the catchment group that it is located in. This ensures that well–gage pairings follow the natural watershed boundaries, enabling direct comparison of groundwater levels with downstream streamflow.

2.5.3. Step 3: Associate Wells with Nearest Stream Segments

GWBASE then associates each well with its nearest stream reach by computing the minimum distance to all the stream segments in the catchment and recording the closest reach identifier along with its streambed elevation. We use the streambed elevation as the local reference datum we use in Step 6 for elevation-based filtering.

Figure 7 illustrates the nearest-reach association for a sample of wells.

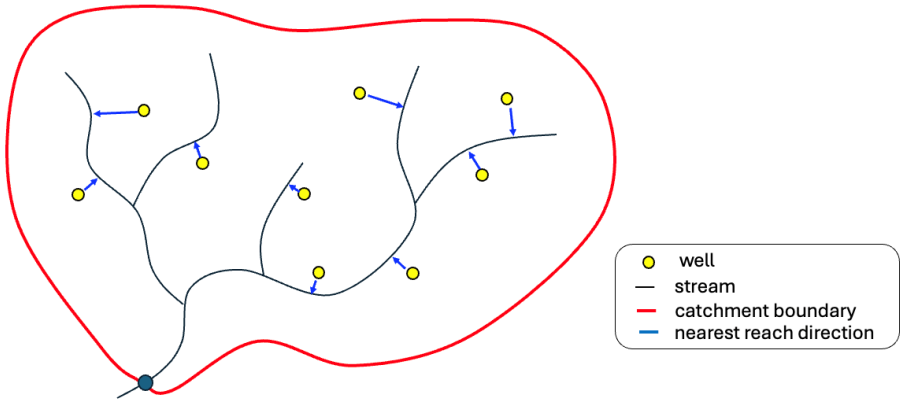

Figure 7. Association of each well with its nearest stream segment, shown for a sample of wells. The recorded streambed elevation of the nearest reach supports the elevation-based filtering in Step 6.

2.5.4. Step 4: Filter Wells with Insufficient Data

Groundwater level observations occur at irregular intervals—some wells monthly, others quarterly, and some with highly variable timing—so records must be filtered to ensure reliable interpolation. The workflow first removes spurious values from each series

and then applies a threshold for the measurement count and record duration each well must meet to identify suitable wells.

GWBASE uses three criteria. First, within each well, a 3 × IQR outlier filter [35] removes extreme values likely to reflect measurement error. This approach is preferred to Z-score filtering because WTE distributions are often skewed, and quantile-based methods may incorrectly flag genuine drought lows as outliers. Second, wells with fewer than 20 observations are excluded. Third, wells with less than three years of record are excluded to ensure sufficient temporal coverage for meaningful interpolation and comparison with streamflow.

2.5.5. Step 5: Temporal Interpolation of Groundwater Levels

GWBASE interpolates groundwater-level time series to monthly resolution using the Piecewise Cubic Hermite Interpolating Polynomial (PCHIP) method [36]. PCHIP is shape-preserving: it honors the monotonic trends between observations and avoids the unrealistic oscillations, such as overshoots or undershoots, that traditional cubic splines can introduce. For each well, observation dates are converted to numerical time, the PCHIP function is fitted to the measurements, and values are computed at monthly intervals across the well's period of record. The resulting interpolated series is combined with the well metadata to produce a dataset with consistent monthly records for comparison with the streamflow records.

2.5.6. Step 6: Elevation-Based Filtering

GWBASE then applies an elevation-based screening criterion to retain only wells with realistic potential for groundwater–surface water interaction. For each well, the mean interpolated WTE is compared against the streambed elevation of its nearest reach (recorded in Step 3). Wells are excluded if the mean WTE lies more than 30 m below that streambed. The reasoning is hydraulic: where the water table sits well below the bottom of the stream, the saturated zone is effectively disconnected from the channel and cannot sustain baseflow to it, so such wells carry little information about groundwater–baseflow coupling. The 30 m cutoff is a practical bound on this effect, consistent with the drop-off in well density and the increasingly confined or poorly connected aquifer settings encountered at greater depths [22,23]. Wells at or above the streambed, and those within 30 m below it, are retained. The 30 m value was a subjective choice based on our experience with the code.

Figure 8 provides a conceptual illustration of this filter.

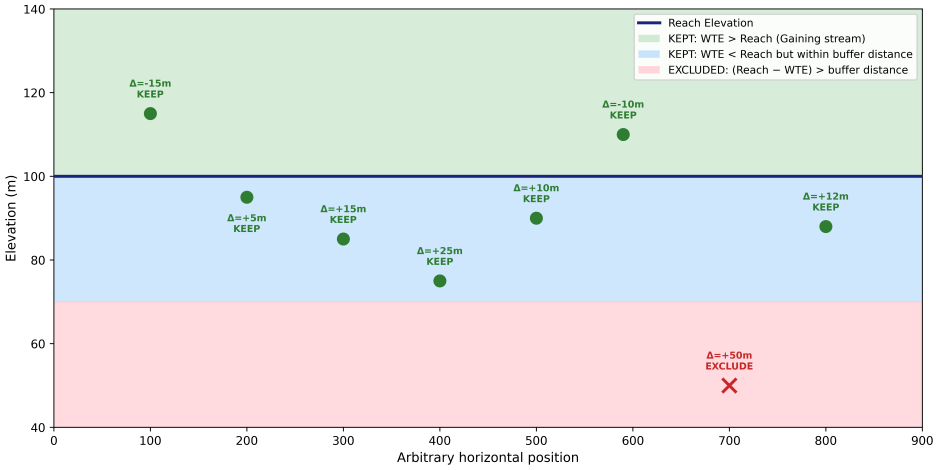

Figure 8. Conceptual illustration of the one-sided, elevation-based well filter. The blue line represents the streambed elevation at the gage; wells lying above the streambed or within 30 m below it (blue and green zones) are retained, while wells whose mean WTE is more than 30 m below the streambed (red zone) are removed.

2.5.7. Step 7: Pair Groundwater and Streamflow Records Under BFD Conditions

GWBASE aggregates daily streamflow to monthly resolution by averaging only days classified as BFD flow (BFD = 1). We excluded months with no BFD days. For each retained month, we pair the interpolated monthly WTE with the corresponding monthly mean BFD-only streamflow at the terminal gage. These paired observations represent conditions where streamflow is more likely to be groundwater-influenced. We retained a terminal gage for the paired analysis only if its contributing area contains at least ten valid wells and sufficient temporal overlap exists between its well and streamflow records. We set this minimum at ten wells because the mutual-information and per-unit sensitivity estimates become unstable at smaller samples; in the demonstration basin this criterion excludes the Spanish Fork catchment (seven wells), whose estimates were erratic throughout. The threshold is a tunable quality criterion that may require adjustment in basins of different well density.

2.5.8. Step 8: Compute ΔWTE and ΔQ

For each well–gage pair, we take the water-table elevation WTE_0 and discharge Q_0 of the earliest baseflow-dominated month as the baseline, with subsequent monthly observations expressed as changes relative to this baseline:

$$\Delta\mathrm{WTE} = \mathrm{WTE} - \mathrm{WTE}_0 \tag{1}$$

$$\Delta Q = Q - Q_0 \tag{2}$$

This formulation emphasizes relative change rather than absolute magnitude, allowing comparison across wells and catchments.

Figure 9 illustrates this procedure for an example well–gage pair.

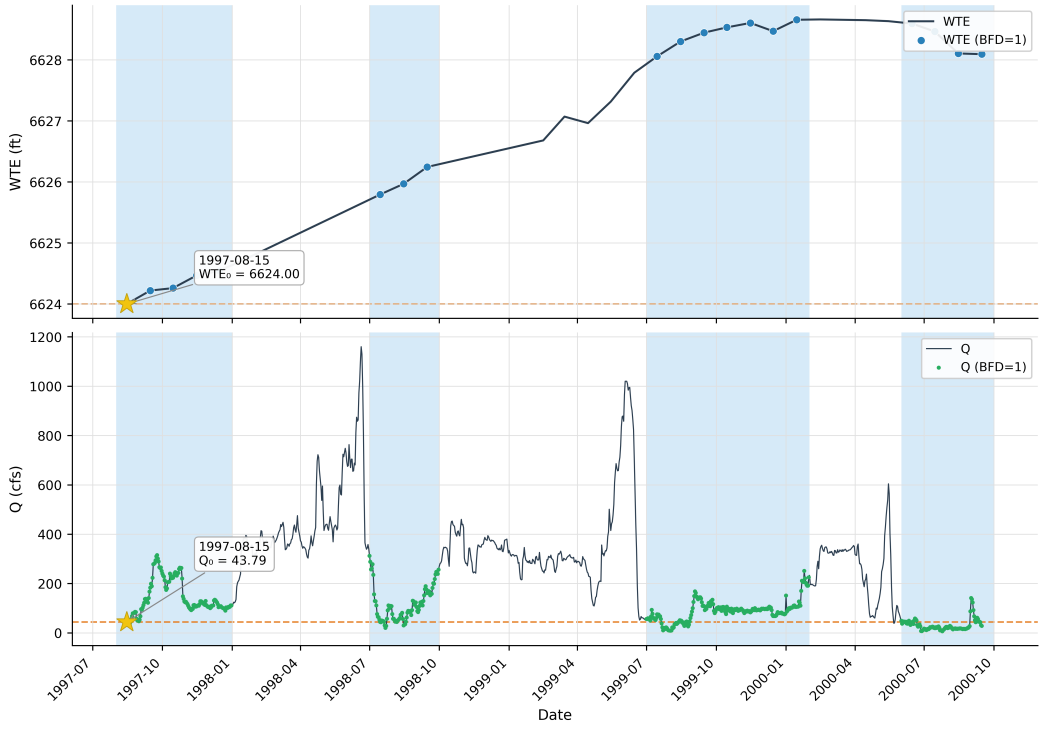

Figure 9. Example groundwater-level (WTE) and streamflow (Q) time series for one well–gage pair, with baseflow-dominated months highlighted; the earliest such month sets the baseline (WTE_0, Q_0), from which ΔWTE and ΔQ for subsequent months are computed. Gold stars mark the baseline month and the orange dashed lines its values; blue points are WTE on baseflow-dominated months and green points are daily Q on baseflow-dominated days.

2.5.9. Step 9: Analyze ΔWTE–ΔQ Relationships

We use linear regression to quantify the relationship between ΔQ and ΔWTE for each well–gage pair, with the slope representing baseflow sensitivity to water-table change and the Pearson correlation coefficient (R^2) indicating strength of linear association. We aggregate these results at the terminal-gage and basin scales to assess the collective, groundwater-driven streamflow coupling and response.

To capture nonlinear relationships, the workflow computes the mutual-information (MI) values [37] between ΔWTE and ΔQ for each well–gage pair. MI quantifies the statistical dependence between two variables without assuming a functional form. Unlike correlation, MI can detect nonlinear and lagged relationships. For two random variables X and Y:

$$I(X;Y) = \sum_x \sum_y p(x,y) \log\left(\frac{p(x,y)}{p(x)p(y)}\right) \quad (3)$$

where $p(x,y)$ is the joint distribution and $p(x)$, $p(y)$ the marginals; zero indicates statistical independence and larger values indicate stronger dependence. MI complements the regression slope where nonlinear coupling is present in the ΔWTE–ΔQ records [38].

For sensitivity testing, GWBASE provides five alternative delta computation methods that remove or bypass the seasonal cycle inherent in the baseline monthly-difference method (Method 1, the monthly-difference method already described in Equations (1) and (2)): (2) annual year-over-year (YoY) differences of annual means; (3) same-quarter YoY differences (year-over-year differencing within each calendar quarter); (4) deseasonalized consecutive-quarter differences (subtracting the long-term quarterly climatology from each quarterly mean, then differencing adjacent quarterly anomalies); (5) rolling 12-month differences (a 12-month trailing mean differenced at a 12-month lag); and (6) standardized anomaly regression on detrended, z-scored monthly series. Section 3.6 compares the six methods, applied to the same well–gage pairs and BFD-filtered records.

3. Results

We apply GWBASE to the GSLB as a case study for demonstration. In this study, the terminal-gage identification algorithm yielded 12 candidate gages (Figure 10).

After data filtering, we retained five of the 12 terminal gages that had sufficient concurrent streamflow and groundwater data for paired analysis: Bear River, Weber River, Spanish Fork, Provo River, and Little Cottonwood Creek. These gages span four of the basin's five named sub-basins (Bear River; Weber River; Spanish Fork and Provo River within Utah Lake; and Little Cottonwood Creek within Jordan River). The West Desert sub-basin retained no qualifying gage. The remaining seven basins were excluded because their catchments contained too few retained wells after quality filtering, lacked sufficient temporal overlap between groundwater and streamflow records, or both. Within the five retained basins, Spanish Fork only has seven wells that passed the screen which falls below the ten-well minimum adopted in Step 7. The Spanish Fork estimates are erratic throughout the analysis and both its mutual-information and per-unit sensitivity values are unstable. Based on these criteria, we excluded it from the catchment rankings and retain it only as a worked illustration of the small-sample failure mode that the threshold guards against. The rankings that follow cover the four remaining catchments (Bear River, 99 wells; Weber River, 106; Provo River, 47; Little Cottonwood Creek, 16).

Table 1 reports the underlying distribution of streamflow and water-table elevation at each terminal gage. These data allow for a more comprehensive understanding of the data, so that the reported regression results in this section can be read against the data they summarize rather than inferred from scatter plots alone.

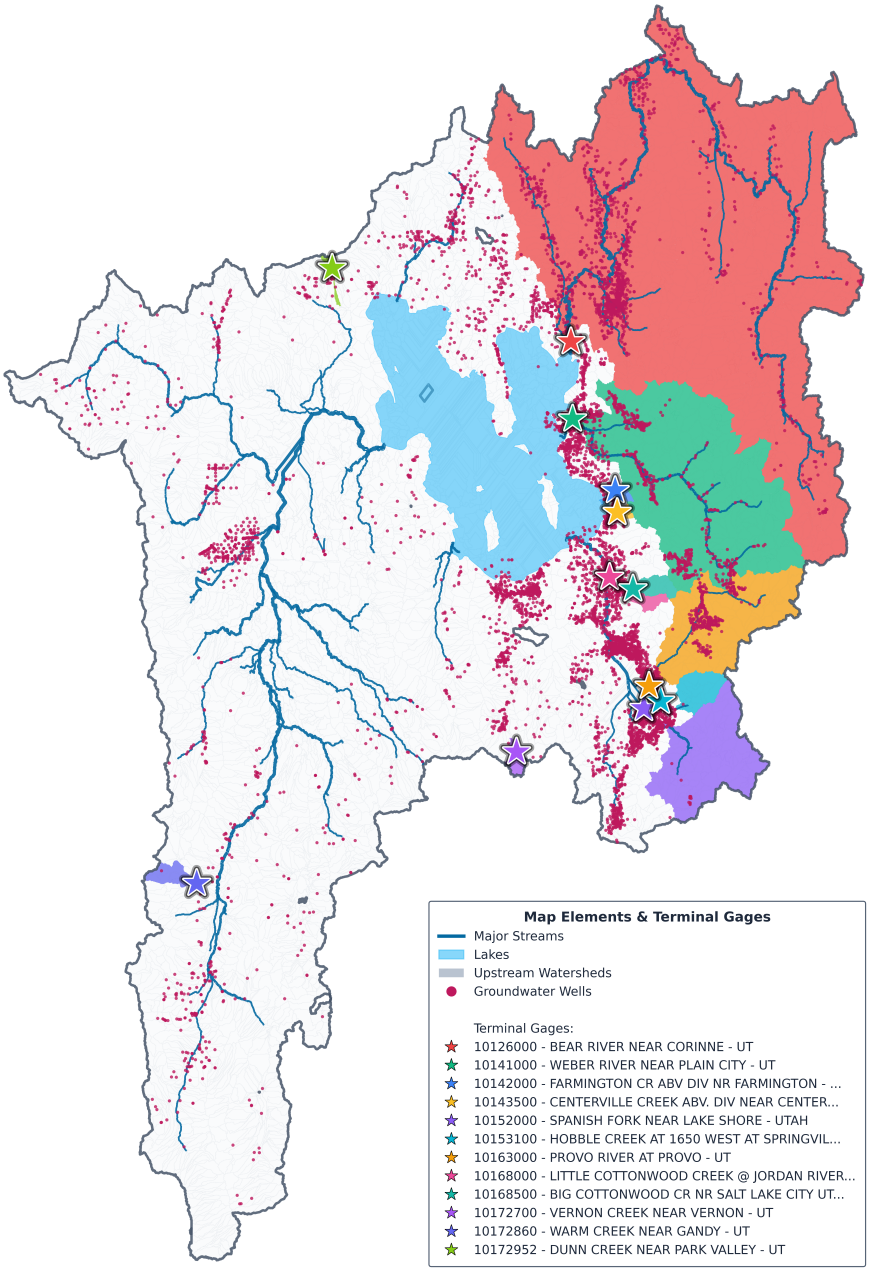

Figure 10. Terminal gages and monitoring network in the GSLB. Colored stars indicate the 12 terminal gage locations, each color-matched to its upstream watershed (shaded polygon); small magenta dots show individual groundwater wells. As in Figure 3, GEOGLOWS routing continuations that crossed the lake polygon have been masked except for the genuine Bear River Bay outlet reach.

While the data summaries may imply hydrologic or topological features, some of the data are misleading. For example, the Bear River's much larger discharge reflects its drainage area rather than a methodological difference and the Provo River's higher water-table elevations reflect local land-surface elevation rather than a deeper or shallower aquifer. We report the Spanish Fork's distributions for completeness but, as noted, we do not use them in the catchment rankings.

We use the Bear River watershed as the initial worked example, because it has the most wells and the longest records. We first examine the groundwater–streamflow coupling at Bear River and then compare results across the retained terminal gages in the watershed. Bear River is the largest tributary to the Great Salt Lake, with a drainage area of approximately 13,000 km^2 and a mix of agricultural, urban, and natural land uses [22]. The

spatial distribution of groundwater wells and the stream network within the watershed are shown in Figure 11.

Table 1. Descriptive statistics of streamflow (Q, cfs) and water-table elevation (WTE, ft) by terminal-gage catchment, from the paired well–month records used throughout this section (1 cfs = 0.0283 m^3/s; 1 ft = 0.3048 m). N_w is the number of contributing wells. WTE statistics are rounded to the nearest foot. IQR and Range are reported as $[Q_1, Q_3]$ and [min, max]. Spanish Fork is shown for completeness but excluded from catchment rankings by the ten-well minimum.

Gage	N_w	n	Mean	Median	IQR	Range
Streamflow, Q (cfs)						
Bear River	99	22,783	677.6	661.0	[245.0, 1002.4]	[40.4, 2140.0]
Weber River	106	18,174	80.9	70.6	[54.8, 97.2]	[1.7, 290.0]
Provo River	47	10,314	102.7	81.9	[37.8, 143.5]	[0.7, 361.5]
Little Cottonwood	16	2479	14.0	10.2	[4.9, 18.3]	[1.0, 64.7]
Spanish Fork	7	1686	64.5	63.9	[12.8, 104.1]	[0.0, 286.3]
Water-table elevation, WTE (ft)						
Bear River	99	22,783	4874	4487	[4422, 4885]	[4232, 6588]
Weber River	106	18,174	5080	4899	[4510, 5138]	[4163, 6875]
Provo River	47	10,314	5898	5641	[5501, 6513]	[4494, 6708]
Little Cottonwood	16	2479	4410	4394	[4311, 4522]	[4248, 4573]
Spanish Fork	7	1686	5040	4593	[4540, 5948]	[4445, 5954]

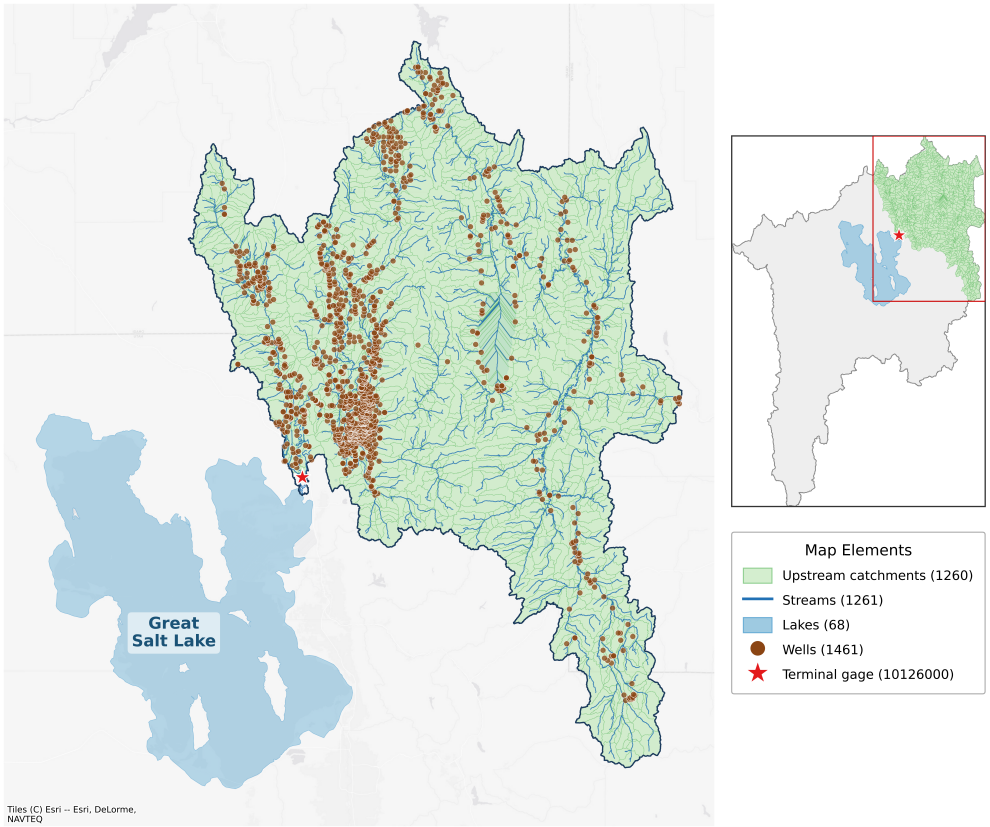

Figure 11. Groundwater wells and the stream network within the Bear River watershed used in the paired analysis.

3.1. Overall ΔWTE–ΔQ Relationships

To quantify the strength and predictability of groundwater–streamflow coupling during BFD periods, we performed linear regression of streamflow change (ΔQ) on water-table elevation change (ΔWTE) across all well–gage pairs.

Figure 12 shows the pooled ΔWTE–ΔQ observations for the Bear River watershed, where each point is a paired monthly observation of water-level change and the corresponding streamflow change during BFD months. The relationship is positive: increases in water-table elevation are associated with increases in streamflow, consistent with groundwater interactions with baseflow.

This pooled monthly-difference regression is the simplest of the constructions we evaluate—the entry point of the method progression developed in Sections 3.6 and 3.7, not the paper's primary estimate—and we present it first because its limitations motivate the refinements that follow. The pooled slope is 5.507 cfs/ft (0.512 $(m^3/s)/m$; $p < 0.001$; Table 2). Following the USGS records' native units, streamflow and slope values are reported in US customary units (cfs, cfs/ft) with SI equivalents in parentheses (1 cfs = 0.0283 m^3/s; 1 cfs/ft = 0.0929 $(m^3/s)/m$; 1 ft = 0.3048 m); tabulated slopes give the SI conversion in the table caption. The very low R^2 (0.002) indicates considerable scatter about the regression line. This low pooled R^2 is structural rather than a sign of absent coupling: pooling every well–month into one scatter makes the total variance dominated by *between-well* differences—two wells in different parts of a heterogeneous basin-fill aquifer register different ΔWTE in the same month—so the denominator of R^2 contains variance the model was never intended to explain. Spatial heterogeneity in aquifer properties and temporal lags between groundwater and streamflow responses contribute further scatter; each of these issues is examined in the subsections that follow, and the between-well component is removed directly in the primary within-well estimate (Section 3.7).

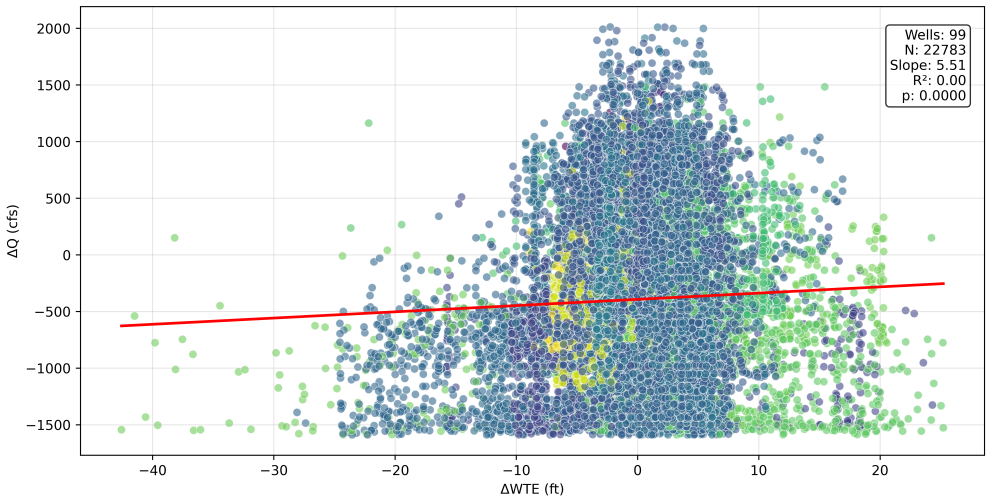

Figure 12. Pooled ΔWTE–ΔQ scatter for all well–gage pairs in the Bear River watershed; each point is one paired monthly ΔWTE–ΔQ observation from a baseflow-dominated month. Point color (viridis colormap) distinguishes the 99 individual contributing wells, each of which supplies multiple points, one per retained month; no legend is drawn, since ninety-nine categories cannot be keyed legibly. Color is included only to show that no single well dominates the pooled cloud. The red line is the pooled ordinary least squares fit.

Table 2. Linear regression summary of ΔWTE–ΔQ relationships by gage. Slopes are in cfs/ft (1 cfs/ft = 0.0929 (m^3/s)/m).

Gage	Gage ID	n_{wells}	n_{obs}	Slope	Intercept	R^2	p-Value
Bear River	10126000	99	22,783	5.507	−393.304	0.002	0.000
Weber River	10141000	106	18,174	0.063	7.270	0.000	0.065
Provo River	10163000	47	10,314	−0.135	46.392	0.000	0.307
Little Cottonwood	10168000	16	2479	0.101	5.408	0.001	0.090

3.2. Seasonal ΔWTE–ΔQ Coupling Patterns

We aggregated the paired observations into four meteorological seasons—Winter (DJF), Spring (MAM), Summer (JJA), and Fall (SON)—pooling enough observations per stratum for stable per-season slope estimates. Figure 13 shows ΔWTE–ΔQ relationships for the Bear River terminal gage (10126000), stratified by season and pooled across contributing wells. All four seasons yield positive slopes (Summer 9.06, Winter 7.74, Spring 6.32, Fall 5.82 cfs/ft; equivalently 0.84, 0.72, 0.59, 0.54 (m^3/s)/m; all $p < 0.01$), and each exceeds the overall pooled slope of 5.507 cfs/ft (Table 2)—a direct sign of the seasonal confounding quantified in Section 3.6, in which pooling across seasons dilutes the coupling strength below that of any single season. The per-season ranking reflects the underlying flow regime. Summer shows the largest slope, consistent with BFD conditions when snowmelt recharge has diminished [21,39] and precipitation is limited, making streamflow at Bear River more directly coupled with groundwater (i.e., the per-unit response to a change in water-table elevation is strongest). The remaining three seasons show weaker but still positive coupling. Winter slopes reflect continued aquifer drainage under low-recharge conditions, whereas Spring and Fall show reduced coupling due to mixed contributions from snowmelt- and precipitation-driven runoff, which are not fully removed by the BFD filter. Given the relatively small differences and the low per-season R^2 values, these seasonal rankings should not be over-interpreted.

3.3. Mutual Information

Mutual information (MI) quantifies statistical dependence without assuming a linear relationship, so it captures nonlinear and lagged coupling. We use MI both as an independent check on the regression-based rankings and to support the lag analysis in Section 3.4. Symmetry differs by metric: MI is symmetric by construction, $I(X;Y) = I(Y;X)$, so every MI result reported here is direction-invariant. Ordinary least squares is not: regressing ΔQ on ΔWTE and ΔWTE on ΔQ give different slopes whose product equals R^2. We report the ΔQ-on-ΔWTE direction throughout because the hypothesized physical direction is groundwater discharge to streamflow; as a check, the reverse-direction regression at Bear River gives a slope of 0.000313 ft/cfs, with the same R^2 (0.002) and p-value ($p < 0.001$) as the forward direction reported in Table 2.

Figure 14 shows the distribution of MI values across well–gage pairs for each terminal gage. Little Cottonwood Creek has the highest median MI and the greatest variability; Bear River, Weber River, and Provo River have lower medians and narrower spreads. The high ranking of Little Cottonwood is consistent with its strong standardized sensitivity and nonlinear dependence. At the within-gage level, the per-pair Spearman correlation between MI and regression-slope magnitude is positive and significant at Bear River ($\rho = +0.36$), Weber River (+0.54), and Little Cottonwood Creek (+0.58; all $p < 0.05$), but not significant at Provo River, indicating that MI and linear regression identify overlapping but not identical sets of coupled pairs.

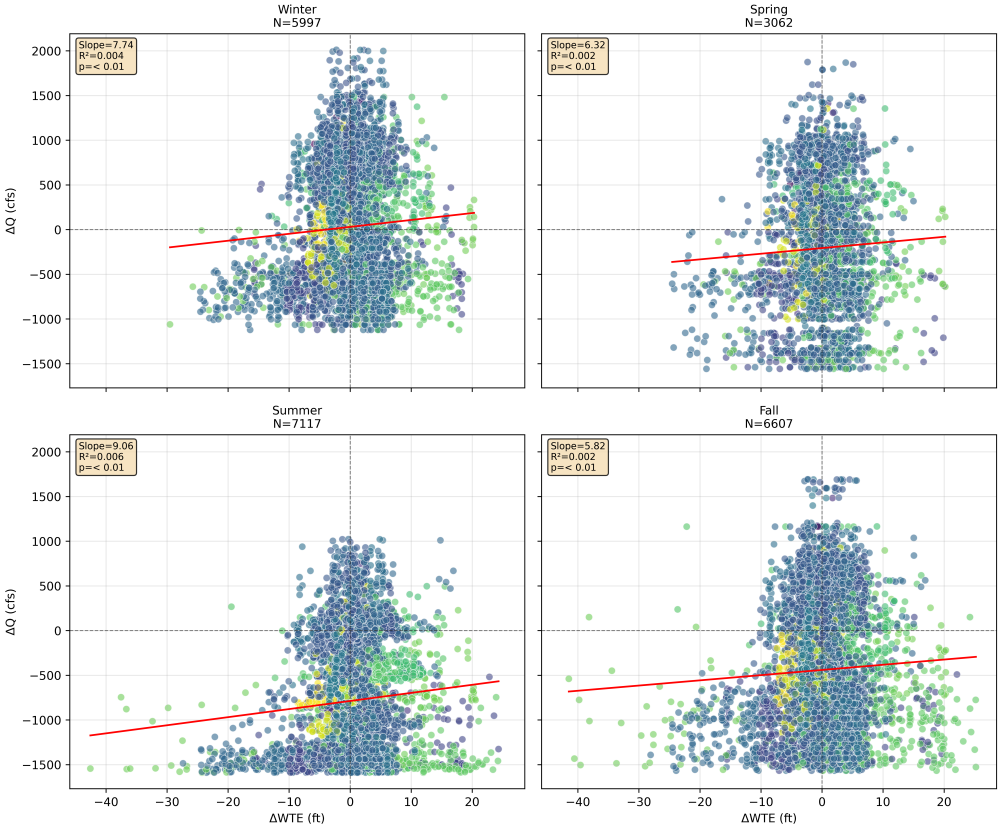

Figure 13. Seasonal ΔWTE–ΔQ scatter at the Bear River terminal gage (10126000) for all contributing well–gage pairs, stratified by Winter (DJF), Spring (MAM), Summer (JJA), and Fall (SON). The red line in each panel is the per-season ordinary least squares fit; inset text reports the pooled slope, R^2, and p-value. Point color (viridis colormap) distinguishes the individual contributing wells, as in Figure 12.

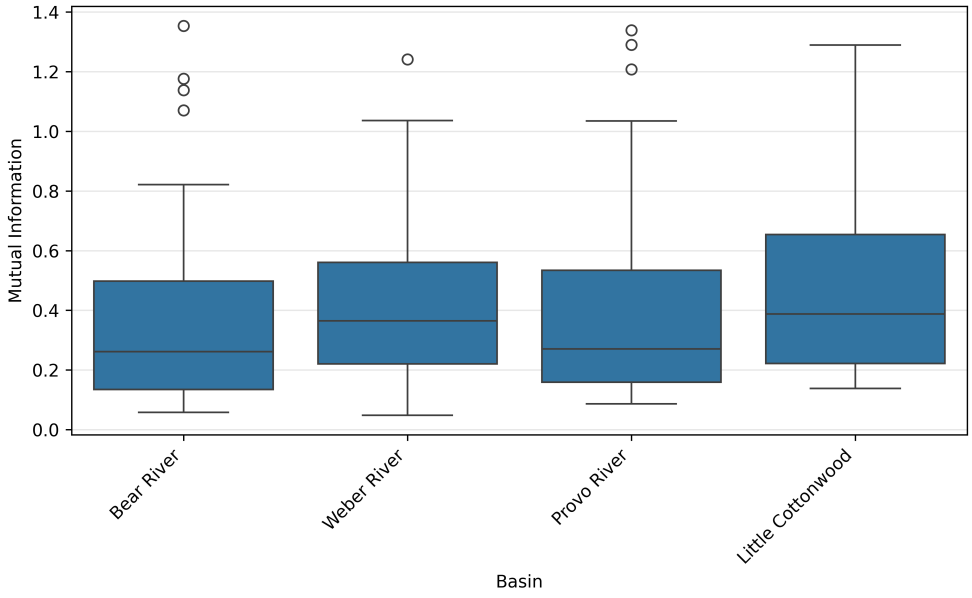

Figure 14. Distribution of mutual-information (MI) values by gage for the four retained GSLB terminal gages. Each box spans the interquartile range of MI scores across wells paired with that gage; the horizontal line is the median; circles are outliers.

To test whether MI detects relationships missed by linear correlation, we compared MI with the absolute Pearson correlation coefficient ($|r|$) for the Bear River terminal gage (Figure 15). Of the 99 well–gage pairs, 98 have valid (non-NaN) values for both MI and $|r|$, so the regression is computed on $n = 98$. The two metrics are positively correlated ($r = 0.311$, $p = 0.0018$), but the scatter is large. Notably, 21 of the 98 pairs (21.4%) show weak linear correlation ($|r| < 0.1$) but above-median MI, indicating substantial nonlinear dependence that linear correlation alone misses. This supports the inclusion of MI as a complementary screening metric: pairs that look uncoupled under linear correlation can still carry meaningful groundwater–streamflow dependence, particularly at the lagged scales examined in the next subsection.

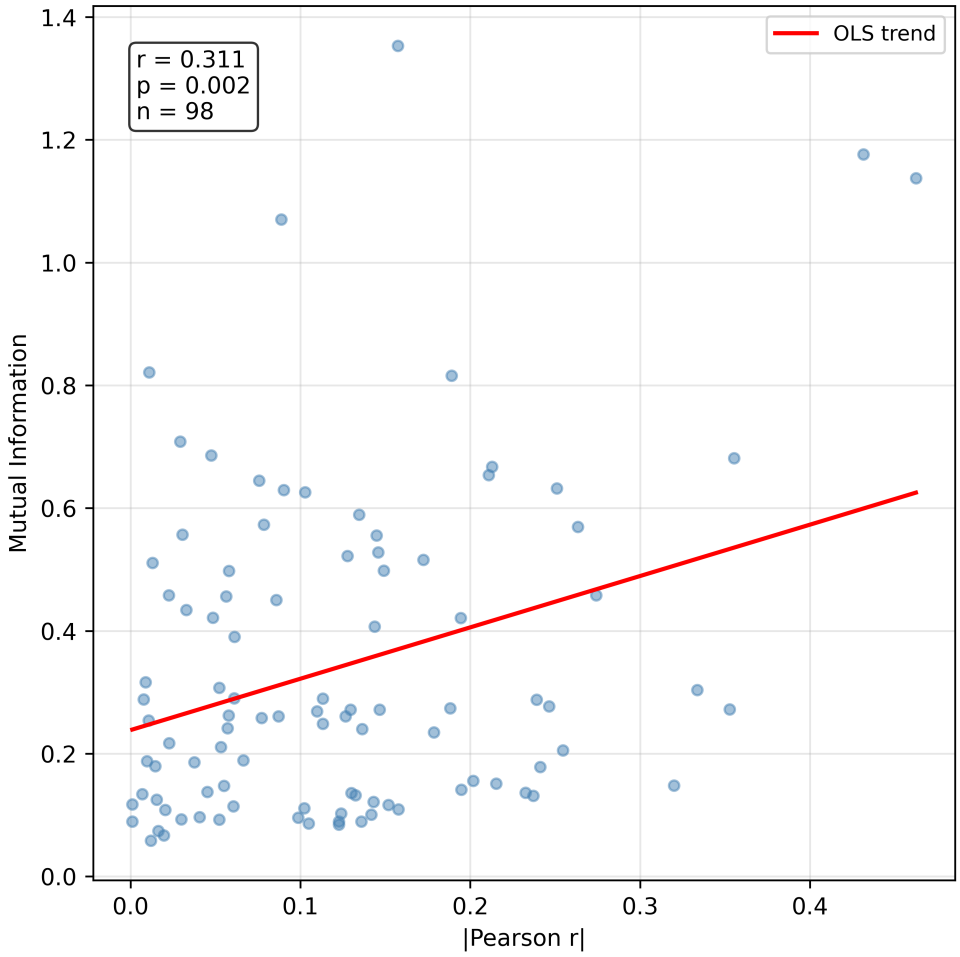

Figure 15. Mutual information (MI) versus absolute Pearson correlation coefficient ($|r|$) for well–gage pairs in the Bear River watershed ($r = 0.311$, $p = 0.0018$, $n = 98$; 98 of the 99 pairs have valid non-NaN values for both metrics). Each blue point is one well–gage pair; the red line is the ordinary least squares trend.

3.4. Lagged Versus Unlagged Coupling Metrics

Because groundwater responses propagate to streams through subsurface pathways with site-specific travel times, distance from the well to the stream, and aquifer diffusivities, groundwater–streamflow coupling may emerge or strengthen at non-zero lag. To test this, we recomputed both R^2 and MI for each well–gage pair after shifting the ΔWTE series so that it precedes ΔQ: a positive lag means that groundwater-level change occurs before the corresponding streamflow response. We tested four discrete lags: 3 and 6 months, to probe

seasonal-scale propagation, and 1 and 5 years, to probe interannual aquifer storage memory. For each gage we report the gain (Δ) of each lagged metric relative to its unlagged baseline.

Figure 16 shows that ΔR^2 is negligible across all gages and lag periods (maximum $\Delta R^2 = 0.0050$ at Provo River, 6-month lag), confirming that any lagged dependence is largely nonlinear and not captured by linear regression. In contrast, ΔMI is consistently positive. Little Cottonwood Creek exhibits the largest increase (peak ΔMI = +0.0497 at the 5-year lag), with Provo River close behind (peak +0.0399, also at a 5-year lag). Bear River and Weber River show smaller but still positive gains (+0.0086 and +0.0203, respectively), also peaking at the 5-year lag. Although these ΔMI values are modest in absolute terms and not subjected to formal significance testing, we use them descriptively, emphasizing the relative differences among gages and the lag at which each peaks rather than the absolute magnitude of the gain.

Read alongside the unlagged MI results (Section 3.3), two patterns emerge. Little Cottonwood is consistent across both views, with the highest unlagged MI and the largest multi-year lag gain, indicating strong and persistent groundwater–streamflow coupling. All four retained gages peak at the 5-year lag, indicating that coupling strengthens over multi-year aquifer-memory timescales at every retained catchment. These results add a *timescale* dimension to the GWBASE screening output: each catchment is characterized not only by coupling strength but by the lag at which that coupling is strongest. This distinction is directly relevant to groundwater management and forecasting, as it identifies whether streamflow responses to groundwater change are expressed over seasonal or multi-year horizons.

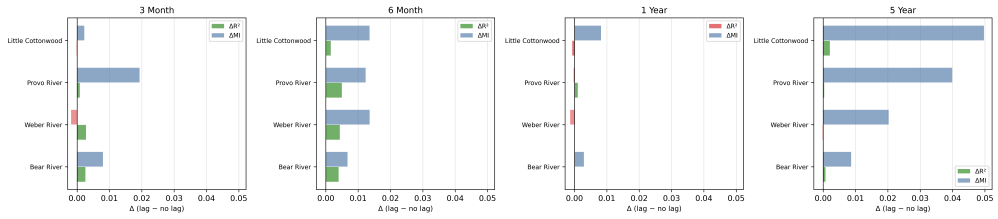

Figure 16. Change in R^2 (ΔR^2, green) and mutual information (ΔMI, blue) relative to the unlagged baseline at four lag periods (3 months, 6 months, 1 year, 5 years) for the four retained GSLB terminal gages. Positive values indicate that the lagged metric exceeds its unlagged counterpart. The ΔR^2 bars are drawn green where the lagged R^2 exceeds the unlagged baseline and red where it falls below; each panel legend shows the color of the ΔR^2 values plotted in that panel.

3.5. Basin-Scale ΔWTE–ΔQ Relationships

Table 2 reports the per-gage regression statistics under the simplest monthly-baseline (Method 1) construction, where each terminal gage's slope (cfs/ft) relates ΔQ to ΔWTE. Bear River (10126000) yields the largest positive slope (5.507 cfs/ft) and is the only gage statistically significant under this construction; Weber River (10141000) and Little Cottonwood Creek (10168000) are small and positive; Provo River (10163000) shows a small negative slope. R^2 values are uniformly $\leq$0.002, so this analysis is best interpreted as ranking catchments by coupling *direction and sensitivity*, rather than explaining variance.

The small negative at Provo River, and the result that indicates only Bear River reaches significance, are artifacts of the simplest construction rather than genuine features of the coupling: Method 1 retains the seasonal cycle, and its pooled slopes absorb between-well baseline differences (Section 3.7). The other sensitivity analysis methods (Section 3.6) show that all five gages return positive slopes under methods that remove or bypass the seasonality (Methods 2–6), and the primary seasonally corrected, within-well estimate (Section 3.7) returns positive slopes at all four catchments, three of them significant. We report Table 2 as the baseline that motivates those refinements, not as the primary result.

Figure 17 shows the ΔWTE–ΔQ scatter for the terminal gages overlaid on a single plot, with per-gage OLS fits and the joint basin regression under the simplest construction. Bear River dominates the scatter due to its large drainage area and discharge magnitude, while Provo River shows the slightly negative per-gage slope noted above, reflecting seasonal confounding and between-well pooling rather than genuine inverse coupling.

Because the terminal-gage catchments differ markedly in drainage area, the raw cfs/ft slopes are scale-dependent and dominated by catchment size rather than intrinsic coupling intensity. To enable comparison across catchments, we instead regress the fractional discharge anomaly on ΔWTE, with each observation's ΔQ normalized by its pairing-time baseline discharge $Q_{0,i}$:

$$\frac{\Delta Q_i}{Q_{0,i}} = \tilde{\beta}_i \cdot \Delta\mathrm{WTE}_i + \varepsilon_i \tag{4}$$

The normalized slope $\tilde{\beta}_i$ (ft^{-1}) represents the fractional change per foot of water-table change, independent of each catchment's absolute discharge magnitude. Computed under the primary within-well specification, the per-gage normalized slopes (Figure 18) for the four catchments are $+0.0066$ ft^{-1} at Bear River, $+0.0034$ ft^{-1} at Weber River, $+0.0138$ ft^{-1} at Provo River, and $+0.124$ ft^{-1} at Little Cottonwood Creek (in SI, $+0.022$, $+0.011$, $+0.045$, and $+0.407$ m^{-1}, respectively; 1 ft^{-1} = 3.281 m^{-1}). Little Cottonwood Creek is the most sensitive on a per-unit basis by a wide margin—its normalized response is roughly nine times the next catchment ($p < 0.001$), whereas the normalized slopes at Bear River and Provo River are not statistically significant. This reverses the raw-slope ranking: Bear River dominates in absolute terms because it is the largest catchment, but the smaller Little Cottonwood Creek emerges as the most groundwater-sensitive when the response is scaled by discharge.

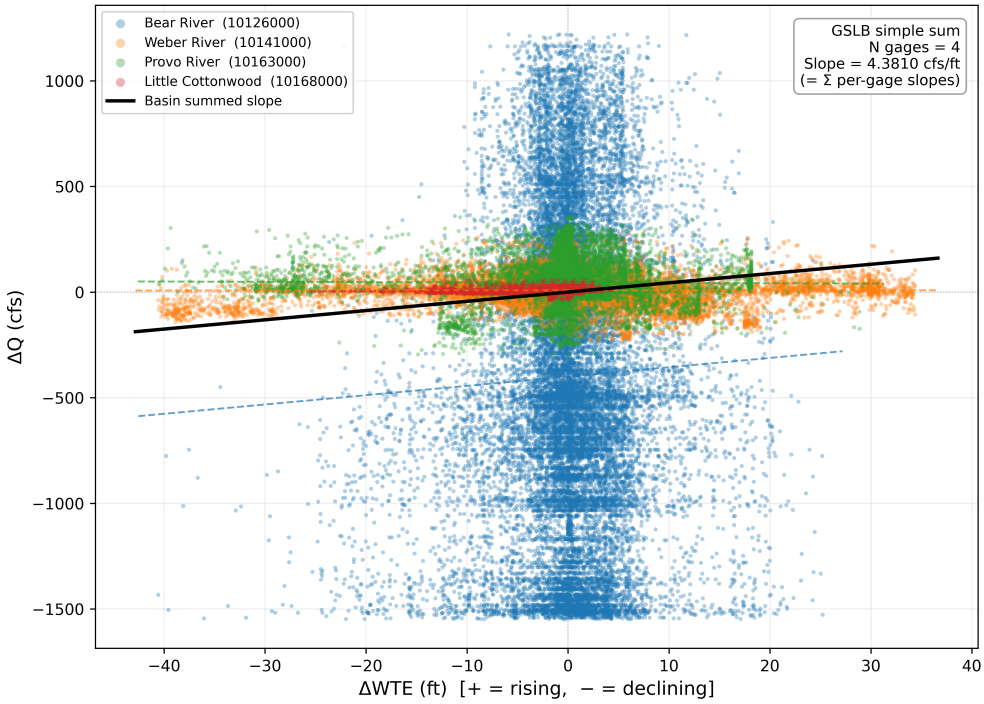

Figure 17. ΔWTE–ΔQ scatter plot for the four retained GSLB terminal gages under the baseline construction. Colored points and dashed lines indicate per-gage data and OLS fits; the solid black line is the basin-sum regression after joint 99th-percentile outlier clipping. The vertical striping visible within each gage's point cloud reflects the coarse (monthly) temporal resolution of the underlying data: PCHIP interpolation between sparse field measurements produces near-linear segments, so a given well's ΔWTE changes little from month to month while ΔQ varies substantially, stacking points into near-vertical columns (Section 4.4).

The per-unit view resolves to a single most-sensitive catchment. It has two facets—response *magnitude* (the normalized slope) and response *tightness* (how little scatter surrounds the relationship, measured by the standardized anomaly slope of Method 6, equivalent to the Pearson correlation of a z-scored series). Among the four catchments, both measures indicated Little Cottonwood Creek is most tightly coupled to groundwater levels: it has the largest normalized slope and the highest standardized anomaly slope (0.28, versus 0.10 at Provo River, 0.08 at Weber River, and 0.05 at Bear River). MI values, which also capture nonlinear dependence, likewise rank Little Cottonwood highest (Section 3.3). The three per-unit measures thus converge, identifying Little Cottonwood Creek as the catchment with the strongest and most reliable groundwater–baseflow coupling—in contrast to the absolute ranking, which is led by Bear River purely through its size.

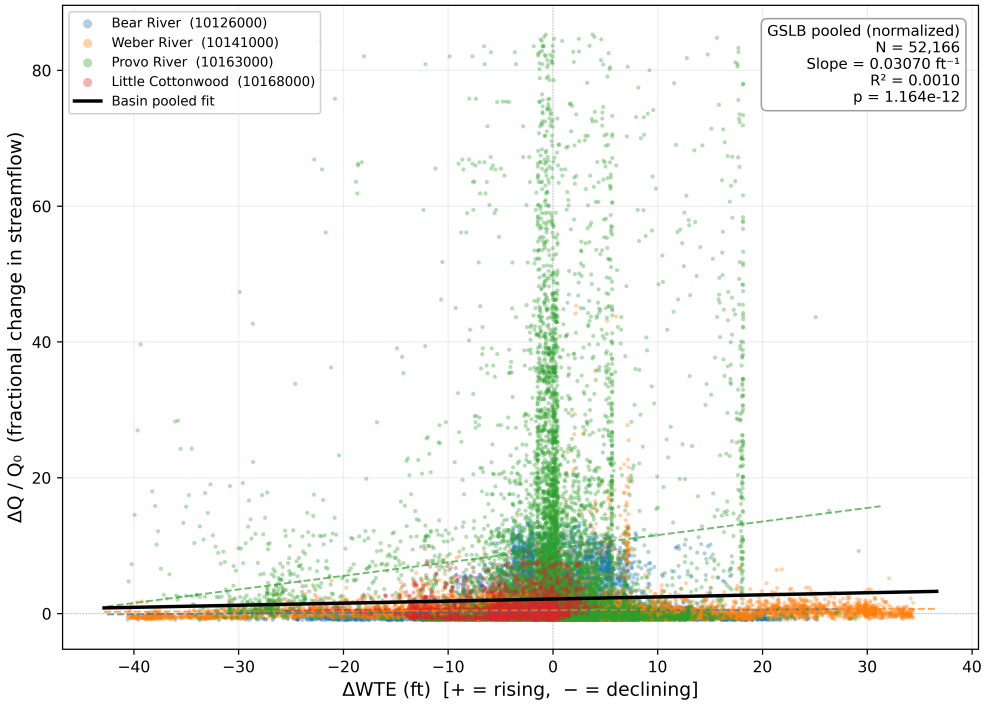

Figure 18. Normalized ΔWTE–ΔQ slopes for GSLB terminal gages. For each well–gage pair, ΔQ is divided by the pairing-time baseline discharge $Q_{0,i}$ (the streamflow at the first BFD $=$ 1 month) to express groundwater sensitivity as a fraction of baseline streamflow, enabling scale-independent comparison across catchments. Colored dashed lines are the per-gage ordinary least squares fits, keyed by gage in the legend; the solid black line is the basin-pooled fit.

Finally, the per-catchment slopes can be summed across the non-overlapping terminal-gage catchments to give a basin-aggregate sensitivity:

$$S_{\text{basin}} = \sum_{i=1}^{N} \hat{\beta}_i \tag{5}$$

where $\hat{\beta}_i$ is the per-catchment slope for gage i and $N = 4$. Under the primary within-well specification, the basin sum is $+3.95$ cfs/ft (0.367 (m^3/s)/m), with a 95% confidence interval of $[-2.00, +9.90]$ cfs/ft propagated from the per-catchment uncertainties. We report this figure only as a rough order-of-magnitude summary, for two reasons. First, roughly 57% of the sum—and nearly all of its confidence-interval width—comes from Bear River, whose own slope is not statistically significant, so the aggregate is close to a Bear River statistic carrying a basin label. Second, and consequently, the interval crosses zero: once catchment-level uncertainty is propagated to the basin scale, the basin sum is not statistically

distinguishable from zero. The coherent unit of analysis is the individual catchment, and we direct readers to the per-catchment rankings above rather than to a single basin-scale coefficient. This matches the physical reality that the GSLB is a collection of largely independent sub-basins, each with its own aquifer and streamflow response characteristics.

3.6. Sensitivity of ΔWTE–ΔQ Coupling Estimates to Computation Method

Because the baseline Method 1 retains the full seasonal cycle, and groundwater levels and streamflow in the GSLB share strong seasonal forcing from snowmelt, diversions, irrigation, and evapotranspiration [21], we compare it against the five alternative delta computation methods described in Section 2. We used the same well–gage pairs and BFD-filtered records. We run pooled OLS regression per well–gage pair under each method; Table 3 reports the gage-level statistics.

Table 3. Pooled ΔWTE–ΔQ OLS regression statistics across six differencing methods for the four retained GSLB terminal gages. Slope units are cfs/ft (1 cfs/ft = 0.0929 (m^3/s)/m) for Methods 1–5; Method 6 slope is dimensionless (σ_Q/σ_{WTE}, marked †). N_w: number of contributing wells; n_{obs}: pooled observation count. p-values ≤ 0.001 are shown as <0.001.

Method	Gage	n_{obs}	N_w	Slope	R^2	p-Value
(1) Monthly Δ (baseline)	Bear River	22,783	99	5.507	0.0017	<0.001
	Weber River	18,174	106	0.063	0.0002	0.065
	Provo River	10,314	47	−0.135	0.0001	0.307
	L. Cottonwood	2479	16	0.101	0.0012	0.090
(2) Annual Δ (YoY)	Bear River	1611	97	10.567	0.0088	<0.001
	Weber River	1332	100	−0.019	0.0000	0.910
	Provo River	847	46	3.527	0.0204	<0.001
	L. Cottonwood	204	15	0.721	0.0860	<0.001
(3) Same-qtr. YoY Δ	Bear River	3960	98	9.436	0.0094	<0.001
	Weber River	3113	102	0.254	0.0016	0.026
	Provo River	2322	47	1.806	0.0090	<0.001
	L. Cottonwood	604	15	0.391	0.0131	0.005
(4) Deseas. consec. qtr.	Bear River	3886	98	4.941	0.0019	0.007
	Weber River	2563	102	0.126	0.0002	0.473
	Provo River	2181	46	0.348	0.0005	0.296
	L. Cottonwood	592	16	0.809	0.0345	<0.001
(5) Rolling 12-month Δ	Bear River	4835	66	5.306	0.0074	<0.001
	Weber River	3600	85	0.464	0.0081	<0.001
	Provo River	3688	41	1.743	0.0077	<0.001
	L. Cottonwood	1004	14	0.563	0.0575	<0.001
(6) Stand. anomaly †	Bear River	22,720	99	0.050	0.0025	<0.001
	Weber River	18,076	106	0.078	0.0062	<0.001
	Provo River	10,265	47	0.095	0.0088	<0.001
	L. Cottonwood	2463	16	0.279	0.0809	<0.001

Three patterns emerge. First, sign consistency depends on seasonal treatment. The baseline monthly-difference approach (Method 1), which retains the full seasonal cycle, produces a negative slope for Provo River (−0.135 cfs/ft, −0.013 (m^3/s)/m; $p = 0.307$). The negative sign is a seasonal artifact: spring snowmelt drives peak streamflow at these gages when WTE has not yet recovered from winter depletion, reversing the pooled monthly regression sign. However, the alternative methods (Methods 2–6), which remove or bypass seasonality in different ways, yield consistently positive slopes across all gages, indicating that the negative slopes in Method 1 reflect seasonal confounding rather than a genuine inverse groundwater–streamflow relationship.

Second, slope magnitude varies systematically with timescale. Year-over-year approaches (Methods 2 and 3) return larger slopes, particularly at Bear River (10.6 and 9.4 cfs/ft; 0.98 and 0.87 $(m^3/s)/m$), than the monthly baseline (5.5 cfs/ft; 0.51 $(m^3/s)/m$), because they isolate interannual groundwater storage variability while reducing intra-annual noise. In contrast, consecutive-quarter anomaly differencing (Method 4) returns weaker and often non-significant relationships—not significant for Weber River or Provo River—suggesting that short-timescale anomaly transitions capture less coherent groundwater–streamflow coupling than year-over-year comparisons at the same season.

Third, explained variance remains uniformly low across all six methods ($R^2 \leq 0.086$), indicating that the weak predictive power is not a methodological artifact but instead reflects intrinsic spatial heterogeneity in the multi-well pooled framework. We expect this is because many of the wells do not represent groundwater aquifers that are connected to streamflow. The comparison shows why no single differencing method serves as a defensible primary estimate on its own: the schemes that most cleanly remove seasonality do so at a cost to statistical inference. The rolling 12-month method (Method 5), for example, applies a 12-month moving average before differencing, so consecutive monthly values share eleven of their twelve underlying months; the resulting serial correlation drives its pooled p-values to essentially zero at every gage, which is the signature of non-independent observations rather than of an unusually strong signal. Rather than elevate one differencing scheme, we remove the two confounding processes that this comparison identifies—the retained seasonal cycle, and the pooling of well–months across wells—directly, and adopt the resulting seasonally corrected, within-well regression as the primary specification (Section 3.7).

3.7. Primary Coupling Estimate: Seasonally Corrected, Within-Well Regression

The method comparison above isolates two properties a defensible primary estimate requires. First, the sign and significance of the coupling depend on whether the seasonal cycle is removed: the simplest construction retains it (Method 1) and returns negative or non-significant slopes at three of five gages, whereas the schemes that remove or bypass seasonality (Methods 2–6) return positive slopes at every retained catchment, with the single exception of a negligible, non-significant -0.019 cfs/ft at Weber River under Method 2. Second, the pooled regressions reported above treat every well–month as an independent observation, which conflates two distinct sources of variation: how streamflow responds to water-table change *within* a well over time, and how wells *differ* from one another in baseline water-table elevation. Because ΔQ at a gage derives from a single discharge series shared by all of that gage's wells, a pooled slope can be dominated by between-well differences rather than by the temporal coupling of any given well to the streamflow.

We adopt as the primary analysis method a seasonally corrected, within-well regression—the simplest method with the two confounding issues removed. For each well we subtract the month-of-year mean from both ΔWTE and ΔQ to remove the annual cycle, and we estimate a single common slope with well fixed effects, so that each well contributes only its own temporal covariation and its baseline elevation cannot influence the fit. Because the ΔQ series is shared across wells within a gage, the pooled observation count overstates the independent information; we cluster standard errors by well, which brings the effective sample size closer to the number of wells than to the number of well–months. Spanish Fork (seven wells) falls below the ten-well minimum adopted in Step 7—its small sample produced unstable estimates throughout the preceding analyses—and is therefore excluded by rule rather than by caveat; the four remaining catchments each contain at least 16 wells.

Table 4 reports the results at zero lag. All four retained catchments return positive slopes, and three of the four are statistically significant; only Bear River is not. This is a marked change from the pooled Method 1 result (Table 2), where Bear River was the sole significant gage and Provo River was negative. The reversal is instructive. Bear River's large pooled slope (5.507 cfs/ft) does not survive the correction, and the two confounding issues act separately. Its apparent significance rested on treating 22,783 correlated well–months as independent: clustering the pooled regression by well, with no other change, widens its 95% confidence interval from $[3.79, 7.23]$ to $[-15.37, 26.38]$. Its magnitude was inflated by between-well variance: estimating within wells on the deseasonalized series lowers the slope to $+2.268$ cfs/ft ($p = 0.42$), with a clustered interval of $[-3.25, 7.79]$. Conversely, Weber and Provo Rivers, non-significant or negative under Method 1, become significantly positive. That the set of significant sites *changes* with the specification, rather than persisting, indicates that these estimates respond to the data rather than to the pooling convention.

Table 4. Seasonally corrected, within-well regression of ΔQ on ΔWTE at zero lag (well fixed effects; standard errors clustered by well). Slopes are in cfs/ft (1 cfs/ft = 0.0929 (m^3/s)/m); the 95% confidence interval is clustered. Spanish Fork is excluded by the ten-well minimum. R^2 is the within-well (fixed-effects) value.

Gage	Gage ID	n_{wells}	Slope	95% CI	R^2	p-Value
Bear River	10126000	99	$+2.268$	$[-3.25, 7.79]$	0.001	0.415
Weber River	10141000	106	$+0.188$	$[+0.03, 0.35]$	0.001	0.018
Provo River	10163000	47	$+0.687$	$[+0.26, 1.11]$	0.004	0.001
Little Cottonwood	10168000	16	$+0.808$	$[+0.57, 1.04]$	0.112	<0.001

Little Cottonwood Creek is the strongest and most robust result: it has the highest within-well R^2 (0.11, roughly two orders of magnitude above the other catchments), the tightest relative confidence interval, and it is the only catchment significant across every lag and specification tested. Its primacy is corroborated independently by the MI analysis (Section 3.3), in which it also ranks highest—two methods indicate on the same catchment is the most coupled. On a per-unit basis (Section 3.5) Little Cottonwood likewise leads, with a size-normalized slope of $+0.124$ ft^{-1} ($p < 0.001$), roughly nine times the next retained catchment. The absolute ranking, by contrast, is led by Bear River purely by virtue of its size, even though its slope is not significant; this divergence between the absolute and per-unit rankings is the reason we report per-catchment screening rather than a single basin coefficient (Section 3.5).

We examined lags of 3, 6, and 12 months in addition to the zero-lag result. The coupling decays with lag rather than peaking at a physical travel time, so we characterize it as contemporaneous coupling within baseflow-dominated months rather than as a lagged travel-time response. We note that the *un*-deseasonalized lag profile oscillates in sign with an annual period—the signature of seasonal phase alignment between two annually cycling series rather than a subsurface response—which is a further reason the seasonal cycle must be removed before the slopes are interpreted.

4. Discussion

4.1. Absolute Strength, Per-Unit Sensitivity, and the Need for Two Metrics

A central diagnostic result is that a catchment's groundwater–baseflow coupling is not captured by a single number, because two easily conflated questions have different answers in the GSLB. The first—which catchment contributes most to the *absolute* basin response—is answered by the un-normalized slope $\hat{\beta}$ (cfs/ft) and is dominated by Bear River through its large drainage area, even though Bear River's own slope is not statistically significant

under the primary specification. This is probably also influenced by the fact that the Bear River watershed has a number of sub-basins, each with their own unique hydrological characteristics. The second—which catchment is most groundwater-sensitive *per unit* of water-table change—is answered by the per-unit measures and points to Little Cottonwood Creek. Both facets of the per-unit view, response magnitude and coupling tightness, identify the same catchment (Section 3.5). The two metrics invert: the catchment that dominates the basin water budget is not the one whose aquifer is most tightly coupled to its stream, and a screening tool that reported only the absolute ranking would mislead a manager asking which catchment is intrinsically most sensitive. This is why GWBASE reports a per-catchment ranking under each metric rather than a single basin-scale coefficient. Table 5 summarizes the two metrics, the question each answers, and the GSLB leader under each.

Table 5. The two coupling metrics GWBASE reports, the question each answers, and the catchment each identifies in the GSLB. Slopes are from the primary within-well specification (Table 4); 1 cfs/ft = 0.0929 $(m^3/s)/m$ and 1 ft^{-1} = 3.281 m^{-1}.

Metric	Symbol (Units)	Question It Answers	GSLB Leader
Absolute coupling magnitude	$\hat{\beta}$ (cfs/ft)	How much total baseflow does this catchment gain or lose per foot of water-table change?	Bear River (size-driven; slope not significant)
Per-unit sensitivity	$\tilde{\beta}$ (ft^{-1}); standardized anomaly slope and mutual information (dimensionless)	What *fraction* of its own baseflow does this catchment gain or lose per foot, and how *reliably* does baseflow track the change?	Little Cottonwood Creek

The same approach applies to how coupling is measured. Linear regression alone systematically understates it: the seasonal cycle retained in the baseline monthly construction dilutes the slope below its per-season values and can even reverse its sign, producing a spurious negative slope at Provo River that disappears once the seasonal mean is removed (Section 3.6). MI is a necessary complement rather than a redundant check: it detects dependence where the Pearson correlation is negligible and resolves the multi-year lagged coupling (Section 3.4) that linear regression cannot. Robust catchment-scale screening of groundwater–baseflow relationships requires both metrics rather than reliance on either alone.

4.2. Long-Term Trends as Independent Validation

To test whether the diagnosed coupling reflects a real physical process rather than an artifact of the pairing procedure, we examined long-term trends at each terminal gage independently of the ΔWTE–ΔQ regression. We computed Sen's slope [40] of annual mean streamflow and per-well annual mean WTE at each gage. We assessed significance using the Mann–Kendall test [41] ($\alpha = 0.05$)—a non-parametric approach appropriate for hydrological records with gaps or skewed distributions [42]. Because interpolated hydrologic series are serially correlated, which inflates the apparent significance of the standard test, we assess significance using the autocorrelation-robust (Hamed–Rao) modification of the Mann–Kendall test [43]; this reduces the number of wells with statistically significant water-table trends (210 of 266 under the plain test to 156 of 266 under the robust test; declining wells fall from 113 to 80) but does not change the direction of the trends. Bear River, Provo River, and Little Cottonwood Creek show statistically significant declining streamflow trends (Bear River the largest, at approximately -2.0 cfs/yr, or -0.057 $m^3/s/yr$); Weber River shows a significant increasing trend ($\approx$+0.4 cfs/yr, +0.011 $m^3/s/yr$). Water-table

trends are predominantly negative across the wells paired with Bear River, Provo River, Little Cottonwood Creek, and Weber River.

These independent trends are consistent with the per-catchment coupling rankings. At Bear River, Provo River, and Little Cottonwood Creek, declining water tables paired with positive ΔWTE–ΔQ coupling are consistent with the multi-decadal streamflow decline. Provo River is the most illustrative case: its coupling is positive only once the seasonal cycle is removed (Methods 2–6; Section 3.6), so the observed water-table–streamflow co-decline is consistent with the interpretation that its negative Method-1 slope is a seasonal artifact rather than a genuine inverse relationship. Weber River's divergence—falling water tables but rising streamflow—is consistent with its near-zero coupling across the computation methods, suggesting that local groundwater storage is not the dominant control on its streamflow. That the coupling inferred from short-term BFD-filtered pairs aligns with independent decadal trends at three of the four retained gages supports the interpretation that GWBASE detects a physical hydrologic association rather than a statistical artifact of the pairing procedure.

4.3. Management Implications

The seasonal and lag structure of the coupling has direct management relevance. At Bear River, ΔWTE–ΔQ coupling is strongest in summer, when streamflow is most baseflow-dominated; groundwater withdrawals in that window coincide with the period when the marginal impact on baseflow per unit of drawdown is greatest. The multi-year lag at which dependence peaks (Section 3.4) further implies that the baseflow consequences of pumping may persist long after withdrawals are reduced—a storage-memory effect relevant to drought-recovery planning.

At the basin-aggregate scale, summing the four retained per-catchment slopes under the primary specification gives a sensitivity of approximately $+3.95$ cfs/ft (0.37 $(m^3/s)/m$), but with a 95% confidence interval of $[-2.0, +9.9]$ cfs/ft that crosses zero and is dominated by the single Bear River catchment (Section 3.5). We treat this figure as an order-of-magnitude screening estimate rather than a firm management number. For scale, summed BFD-month baseflow across the four gages is roughly 670 cfs, so the point estimate corresponds to about 0.6% of basin baseflow per foot of decline; at the water-table decline rates observed in the basin, the implied multi-decadal reduction remains a small fraction of baseflow. The management-relevant output is the per-catchment ranking—which identifies where, and at what timescale, baseflow is most sensitive to groundwater change—rather than a single basin coefficient.

4.4. Limitations and Transferability

Several limitations bound the interpretations made in this study. Explained variance is uniformly low ($R^2 \leq 0.086$ across all six pooled methods), which follows from pooling many heterogeneous wells against a single gage record and is the reason we adopt a within-well primary specification (Section 3.7); even so, GWBASE is best understood as a screening tool that ranks catchments by coupling direction, sensitivity, and dependence, not as a predictive model of baseflow. Spanish Fork retains only seven wells and falls below the ten-well minimum; we exclude it from the rankings and report it only as an illustration of the small-sample failure mode, in which both its normalized slope and its mutual information become unstable.

The analysis does not screen groundwater wells by aquifer type, screened interval, confinement, or flowing-artesian condition. We examined the USGS expanded site records for the study wells and found that the attributes needed for such screening are too sparsely populated to serve as filters at a regional scale—only about 12% of wells carry a con-

fined/unconfined designation, and screened-interval data are largely absent—while deep completions and confined wells are demonstrably present in the sample. More fundamentally, demonstrating hydraulic connectivity between a specific well completion and a specific reach cannot be established from national datasets; it requires site-specific hydrogeologic investigation. GWBASE identifies catchments whose observations are *consistent with* groundwater–baseflow coupling and flags them as candidates for the site-specific investigation that would establish it, rather than confirming connectivity directly. The elevation-based filter (Step 6), the well-to-reach distance, and the streambed-offset criterion bound, but do not verify, topographic and lithostratigraphic connection.

The monthly resolution sets the timescale the method can resolve. Groundwater levels in the national network are predominantly intermittent manual measurements, so interpolating finer than monthly would manufacture a structure the observations do not contain; a daily, event-scale analysis is not feasible in this basin, where only three continuous recorders in the terminal-gage catchments carry ten or more years of record and two of the catchments have none. GWBASE as implemented resolves seasonal-to-interannual storage coupling rather than event-scale exchange, consistent with the multi-year lag at which mutual information peaks (Section 3.4). Relatedly, a month is retained if it contains any baseflow-dominated day, so months built from few such days carry more noise than fully baseflow-dominated months—a limitation of the monthly BFD aggregation.

Terminal-gage identification still requires a manual review step to correct diversions, shared outlets, and straddling divides, which limits full end-to-end automation. The quality thresholds—a 30 m streambed offset, and minimums of ten wells per catchment, 20 observations, and three years of record—were tuned to the GSLB and may require adjustment in basins with different well densities or hydrogeology. Finally, the workflow depends on an externally trained machine learning classifier to label baseflow-dominated days (Section 2.4), which has a known tendency to over-include days at the onset of rain-driven events; a sensitivity test that drops the third of BFD days most exposed to this error shifts the slopes by only a small amount without changing their sign, but the classifier's portability to new regions is contingent on its remaining valid there.

These caveats notwithstanding, GWBASE relies only on USGS groundwater and streamflow records and GEOGLOWS hydrography, so it can be applied to other basins without additional data collection. Its configurable thresholds and alternative delta computation methods let users probe sensitivity and adapt the workflow to different data densities and hydrologic settings.

5. Conclusions

GWBASE provides a transferable, observation-based way to screen the catchments of a region and identify where stream baseflow is groundwater-influenced, using only existing USGS well and gage records together with GEOGLOWS hydrography. Applied to the Great Salt Lake Basin, it ranks the retained catchments by two complementary metrics: by *absolute* coupling magnitude, Bear River dominates the basin response through its large drainage area, whereas by size-normalized, *per-unit* sensitivity—and by coupling tightness and MI—the smaller Little Cottonwood Creek emerges as the most groundwater-sensitive catchment. Distinguishing these metrics—using a seasonally corrected, within-well regression to quantify the magnitude and direction of coupling, and MI to capture the nonlinear, lagged dependence that regression misses—is the primary contribution of the method.

The groundwater–baseflow coupling is nonlinear, seasonally structured, and operates over month-to-year timescales, so robust screening requires both metrics rather than either alone; independent multi-decadal water-table–streamflow co-declines are consistent with the detected coupling being physical rather than a statistical artifact of the pairing procedure.

A basin-scale aggregate sensitivity of about 4 cfs per foot of basin-averaged decline can be formed by summing the per-catchment slopes, but it is dominated by a single catchment and, once catchment-level uncertainty is propagated, is not statistically distinguishable from zero; GWBASE is best applied as a per-catchment screening and ranking tool rather than as a source of a single basin-scale coefficient. Because it requires no new data collection, it can be applied directly to other basins for regional groundwater–baseflow assessment.

Author Contributions: Conceptualization, X.L., N.L.J. and G.P.W.; methodology, X.L., N.L.J., G.P.W. and A.A.; software, X.L. and R.C.H.; validation, X.L.; formal analysis, X.L.; investigation, X.L.; resources, N.L.J.; data curation, X.L.; writing—original draft preparation, X.L.; writing—review and editing, N.L.J., G.P.W., A.A., R.C.H., E.W.-E., R.v.d.H., T.P.C. and D.M.R.; visualization, X.L.; supervision, N.L.J. and G.P.W.; project administration, N.L.J.; funding acquisition, N.L.J. All authors have read and agreed to the published version of the manuscript.

Funding: Funding for this project was provided by the National Oceanic & Atmospheric Administration (NOAA), awarded to the Cooperative Institute for Research to Operations in Hydrology (CIROH) through the NOAA Cooperative Agreement with The University of Alabama (NA22NWS4320003).

Institutional Review Board Statement: Not applicable.

Informed Consent Statement: Not applicable.

Data Availability Statement: The groundwater-level and streamflow observations analyzed in this study are publicly available from the U.S. Geological Survey National Water Information System (NWIS) at https://waterdata.usgs.gov/ (accessed on 28 December 2025). The GWBASE source code, processing pipeline, and analysis notebooks used to generate all results and figures are available at https://github.com/BYU-Hydroinformatics/gwbase (accessed on 26 August 2026) and archived at https://doi.org/10.5281/zenodo.21827996, allowing the analyses presented here to be fully reproduced from the public USGS data.

Acknowledgments: During the preparation of this work, the authors used Claude Code (Anthropic, San Francisco, CA, USA), Opus 5 model to help organize and enhance the GWBASE code and to assist with editing the manuscript. The authors have reviewed and edited the output and take full responsibility for the content of this publication.

Conflicts of Interest: The authors declare no conflicts of interest.

Abbreviations

The following abbreviations are used in this manuscript:

GSLB	Great Salt Lake Basin
WTE	Water-Table Elevation
BFD	Baseflow-Dominated
MI	Mutual Information
USGS	United States Geological Survey
NWIS	National Water Information System
PCHIP	Piecewise Cubic Hermite Interpolating Polynomial
OLS	Ordinary Least Squares
IQR	Interquartile Range
YoY	Year-over-Year
GW–SW	Groundwater–Surface Water

References

1. Winter, T.C.; Harvey, J.W.; Franke, O.L.; Alley, W.M. *Ground Water and Surface Water: A Single Resource*; U.S. Geological Survey Circular 1139; U.S. Geological Survey: Denver, CO, USA, 1998. [CrossRef]
2. Smakhtin, V.U. Low Flow Hydrology: A Review. *J. Hydrol.* **2001**, *240*, 147–186. [CrossRef]

3. Barlow, P.M.; Leake, S.A. *Streamflow Depletion by Wells—Understanding and Managing the Effects of Groundwater Pumping on Streamflow*; U.S. Geological Survey Circular 1376; U.S. Geological Survey: Reston, VA, USA, 2012. [CrossRef]
4. Carroll, R.W.H.; Niswonger, R.G.; Ulrich, C.; Varadharajan, C.; Siirila-Woodburn, E.R.; Williams, K.H. Declining Groundwater Storage Expected to Amplify Mountain Streamflow Reductions in a Warmer World. *Nat. Water* **2024**, *2*, 419–433. [CrossRef]
5. Mukherjee, A.; Bhanja, S.N.; Wada, Y. Groundwater Depletion Causing Reduction of Baseflow Triggering Ganges River Summer Drying. *Sci. Rep.* **2018**, *8*, 12049. [CrossRef]
6. Abbas, S.A.; Bailey, R.T.; White, J.T.; Arnold, J.G.; White, M.J. Estimation of Groundwater Storage Loss Using Surface–Subsurface Hydrologic Modeling in an Irrigated Agricultural Region. *Sci. Rep.* **2025**, *15*, 8350. [CrossRef]
7. Konikow, L.F. Long-Term Groundwater Depletion in the United States. *Groundwater* **2015**, *53*, 2–9. [CrossRef]
8. Jasechko, S.; Seybold, H.; Perrone, D.; Fan, Y.; Shamsudduha, M.; Taylor, R.G.; Fallatah, O.; Kirchner, J.W. Rapid Groundwater Decline and Some Cases of Recovery in Aquifers Globally. *Nature* **2024**, *625*, 715–721. [CrossRef]
9. Famiglietti, J.S. The Global Groundwater Crisis. *Nat. Clim. Change* **2014**, *4*, 945–948. [CrossRef]
10. Scanlon, B.R.; Faunt, C.C.; Longuevergne, L.; Reedy, R.C.; Alley, W.M.; McGuire, V.L.; McMahon, P.B. Groundwater Depletion and Sustainability of Irrigation in the US High Plains and Central Valley. *Proc. Natl. Acad. Sci. USA* **2012**, *109*, 9320–9325. [CrossRef]
11. Hodgkins, G.A.; Dudley, R.W.; Nielsen, M.G.; Renard, B.; Qi, S.L. Groundwater-Level Trends in the U.S. Glacial Aquifer System, 1964–2013. *J. Hydrol.* **2017**, *553*, 289–303. [CrossRef]
12. Rojanasakul, M.; Flavelle, C.; Migliozzi, B.; Murray, E. America Is Draining Its Groundwater Like There's No Tomorrow. *New York Times*, 28 August 2023. Available online: https://www.nytimes.com/interactive/2023/08/28/climate/groundwater-drying-climate-change.html (accessed on 28 May 2026).
13. Barbosa, S.A.; Pulla, S.T.; Williams, G.P.; Jones, N.L.; Mamane, B.; Sanchez, J.L. Evaluating Groundwater Storage Change and Recharge Using GRACE Data: A Case Study of Aquifers in Niger, West Africa. *Remote Sens.* **2022**, *14*, 1532. [CrossRef]
14. Barbosa, S.A.; Jones, N.L.; Williams, G.P.; Teklu, H.; Yidana, S.M.; Pulla, S.T.; Sanchez, J.L.; Nelson, E.J.; Ames, D.P.; Miller, A.W. A Multi-Source Approach to Groundwater Storage and Recharge Assessment in the Volta Basin. *Sci. Total Environ.* **2025**, *1001*, 180421. [CrossRef]
15. Sophocleous, M. Interactions Between Groundwater and Surface Water: The State of the Science. *Hydrogeol. J.* **2002**, *10*, 52–67. [CrossRef]
16. Wittenberg, H. Baseflow Recession and Recharge as Nonlinear Storage Processes. *Hydrol. Process.* **1999**, *13*, 715–726. [CrossRef]
17. Eckhardt, K. How to Construct Recursive Digital Filters for Baseflow Separation. *Hydrol. Process.* **2005**, *19*, 507–515. [CrossRef]
18. Bosch, D.D.; Lowrance, R.R.; Sheridan, J.M.; Williams, R.G. Ground Water Storage Effect on Streamflow for a Southeastern Coastal Plain Watershed. *Groundwater* **2003**, *41*, 903–912. [CrossRef]
19. Aghababaei, A.; Jones, N.L.; Williams, G.P.; Webster-Esho, E.; van der Heijden, R.; Li, X.; Clement, T.P.; Rizzo, D.M. Development and Comparison of Methods for Identification of Baseflow-Dominant Periods in Streamflow Records. *Water* **2025**, *17*, 3083. [CrossRef]
20. Wurtsbaugh, W.A.; Miller, C.; Null, S.E.; DeRose, R.J.; Wilcock, P.; Hahnenberger, M.; Howe, F.; Moore, J. Decline of the World's Saline Lakes. *Nat. Geosci.* **2017**, *10*, 816–821. [CrossRef]
21. Bedford, D.; Douglass, A. Changing Properties of Snowpack in the Great Salt Lake Basin, Western United States, from a 26-Year SNOTEL Record. *Prof. Geogr.* **2008**, *60*, 374–386. [CrossRef]
22. Smith, L.R. *Groundwater Conditions in Utah, Spring of 2018*; Cooperative Investigations Report No. 59; U.S. Geological Survey: Salt Lake City, UT, USA, 2019. Available online: https://pubs.usgs.gov/publication/70203559 (accessed on 28 December 2025).
23. Heilweil, V.M.; Brooks, L.E. *Conceptual Model of the Great Basin Carbonate and Alluvial Aquifer System*; Scientific Investigations Report 2010–5193; U.S. Geological Survey: Reston, VA, USA, 2011. [CrossRef]
24. Utah Division of Water Resources. *Jordan River Basin Planning for the Future*; Utah State Water Plan; Utah Department of Natural Resources: Salt Lake City, UT, USA, 2010. Available online: https://water.utah.gov/wp-content/uploads/2019/SWP/JordanRiver/Jordan-River-Basin-Final2010.pdf (accessed on 28 December 2025).
25. Utah Division of Water Resources. *Utah Lake Basin Planning for the Future*; Utah State Water Plan; Utah Department of Natural Resources: Salt Lake City, UT, USA, 2014. Available online: https://water.utah.gov/wp-content/uploads/2019/SWP/UtahLake/UtahLake2014.pdf (accessed on 28 December 2025).
26. Grineski, S.E.; Mallia, D.V.; Collins, T.W.; Araos, M.; Lin, J.C.; Anderegg, W.R.L.; Perry, K. Harmful Dust from Drying Lakes: Preserving Great Salt Lake (USA) Water Levels Decreases Ambient Dust and Racial Disparities in Population Exposure. *One Earth* **2024**, *7*, 1056–1067. [CrossRef]
27. Young, Z.M.; Kreemer, C.; Blewitt, G. GPS Constraints on Drought-Induced Groundwater Loss Around Great Salt Lake, Utah, with Implications for Seismicity Modulation. *J. Geophys. Res. Solid Earth* **2021**, *126*, e2021JB022020. [CrossRef]
28. Teklu, H.; Jones, N.L.; Williams, G.P.; Sowby, R.B.; Serago, J. Groundwater Storage Trends in the Great Salt Lake Basin, 2002–2024. *JAWRA J. Am. Water Resour. Assoc.* 2026, *submitted*.

29. Hall, D.K.; Loomis, B.D.; DiGirolamo, N.E.; Forman, B.A. Snowfall Replenishes Groundwater Loss in the Great Basin of the Western United States, but Cannot Compensate for Increasing Aridification. *Geophys. Res. Lett.* **2024**, *51*, e2023GL107913. [CrossRef]
30. USGS. USGS Groundwater Data for the Nation. Available online: https://nwis.waterdata.usgs.gov/nwis/gw (accessed on 10 December 2025).
31. GEOGLOWS. Available online: https://www.geoglows.org/ (accessed on 28 December 2025).
32. USGS. Water Data for the Nation. Available online: https://waterdata.usgs.gov/nwis (accessed on 28 December 2025).
33. NOAA Office of Water Prediction. National Water Model. Available online: https://water.noaa.gov/about/nwm (accessed on 28 December 2025).
34. Li, X.; Jones, N.L.; Williams, G.P.; Hales, R.C. *GWBASE: An Algorithm for Screening Groundwater–Baseflow Coupling Using Paired USGS Well and Streamflow Records*; Zenodo: Geneva, Switzerland, 2026. [CrossRef]
35. Tukey, J.W. *Exploratory Data Analysis*; Addison-Wesley: Reading, MA, USA, 1977.
36. Fritsch, F.N.; Carlson, R.E. Monotone Piecewise Cubic Interpolation. *SIAM J. Numer. Anal.* **1980**, *17*, 238–246. [CrossRef]
37. Shannon, C.E. A Mathematical Theory of Communication. *Bell Syst. Tech. J.* **1948**, *27*, 379–423. [CrossRef]
38. Sharma, A. Seasonal to Interannual Rainfall Probabilistic Forecasts for Improved Water Supply Management: Part 1—A Strategy for System Predictor Identification. *J. Hydrol.* **2000**, *239*, 232–239. [CrossRef]
39. Earman, S.; Campbell, A.R.; Phillips, F.M.; Newman, B.D. Isotopic Exchange Between Snow and Atmospheric Water Vapor: Estimation of the Snowmelt Component of Groundwater Recharge in the Southwestern United States. *J. Geophys. Res. Atmos.* **2006**, *111*, D09302. [CrossRef]
40. Sen, P.K. Estimates of the Regression Coefficient Based on Kendall's Tau. *J. Am. Stat. Assoc.* **1968**, *63*, 1379–1389. [CrossRef]
41. Mann, H.B. Nonparametric Tests Against Trend. *Econometrica* **1945**, *13*, 245–259. [CrossRef]
42. Helsel, D.R.; Hirsch, R.M.; Ryberg, K.R.; Archfield, S.A.; Gilroy, E.J. *Statistical Methods in Water Resources*; U.S. Geological Survey Techniques and Methods, Book 4, Chapter A3, version 1.1; U.S. Geological Survey: Reston, VA, USA, 2020. [CrossRef]
43. Hamed, K.H.; Rao, A.R. A Modified Mann-Kendall Trend Test for Autocorrelated Data. *J. Hydrol.* **1998**, *204*, 182–196. [CrossRef]

Disclaimer/Publisher's Note: The statements, opinions and data contained in all publications are solely those of the individual author(s) and contributor(s) and not of MDPI and/or the editor(s). MDPI and/or the editor(s) disclaim responsibility for any injury to people or property resulting from any ideas, methods, instructions or products referred to in the content.